Geodetic and Oceanographic Aspects of Absolute versus Relative Sea-Level Change

Dissertation

Presented in Partial Fulfillment of the Requirements for the Degree Doctor of Philosophy in the Graduate School of The Ohio State University

By

Dana John Caccamise II, M.S.

Graduate Program in Earth Science

The Ohio State University

2018

Dissertation Committee:

Michael G. Bevis, Adviser

C. K. Shum

Loren Babcock

Abstract

Tide gauges record relative sea level (RSL), i.e. the vertical position of the sea surface relative to the adjacent land mass or relative to the seafloor under the gauge. A tide gauge cannot distinguish between a rise in sea level or subsidence of the land or seawall or pier that supports the gauge. Absolute sea level (ASL) refers to the level or height of the sea surface stated in some standard geodetic reference frame, e.g. ITRF2008. Since satellite altimeters make a geometrical measurement of sea level, this constitutes a determination of ASL. Satellite altimeters suffer from instrumental drift and thus need to be calibrated using tide gauges. This requires us to estimate the rate of RSL change at each tide gauge and convert this into an estimate of the rate of ASL change. This is done using a GPS station located at or near the tide gauge, since it can measure the vertical velocity of the lithosphere – often referred to as vertical land motion, VLM – which allows us to exploit the relationship ASL = RSL + VLM. This goal has motivated geodesists to build dozens of continuous GPS (or CGPS) stations near tide gauges – an agenda sometimes referred to as the CGPS@TG agenda. Unfortunately, a significant fraction of all long-lived tide gauges – especially those in the Pacific - have also recorded non-steady land motion caused by earthquakes. Rather than simply delete such datasets from the agenda, this thesis explores a new analytical method, based on the concept of a geodetic station trajectory model, that allows us to compute RSL and ASL rates even at tide gauges

affected by regional earthquakes. We illustrate this method using two tide gauges (PAGO and UPOL) and three GPS stations (ASPA, SAMO and FALE) located in the Samoan islands of the Southwest Pacific. In addition to managing the impact of large regional earthquakes, we also seek new approaches to reducing noise in RSL rate estimates by suppressing the higher frequency sea level changes associated with ocean dynamics. We do this by augmenting our trajectory models using an ocean climate index or using numerical models of the sea surface state.

Dedication

I dedicate this work to Philia, Eros, Agape, Pragma and my dependents “The Most Beautiful Girl (Maia) In the World”, a Prince song and her doggies (Daisy and Buster).

Acknowledgements

I first and foremost would like to acknowledge and extend the greatest loving thanks to my wife Sarah and daughter Maia for their unconditional love and the many accommodations that they have made for me, thus allowing me to pursue and finish these works.

Nobody excels in science alone, and with this in mind, this research was not funded in a traditional way (i.e. government), but by the generous contributions of Michael Bevis's personal research funds.

A heartfelt thanks goes to Michael Bevis (Chair), C.K. Shum, Loren Babcock, Michael Barton, and Terry Wilson for their contributions and willingness to be part of my committee, doctoral research, and for their help and guidance over the years. I would also like to explicitly thank Mark Merrifield, Jacob Heck, and Matthew Widlansky for their assistance with non-trivial issues related to this research.

I am very fortunate to have been able to work and collaborate with friends and colleagues alike; a shout out goes to Eric Kendrick, Fei Wang, Demian Gomez, Peng Feng, Yehuda Bock, David Conner, Mark Schenewerk, Ken Hudnut, Bill Stone, Bob Smalley, Fred

Taylor, Brent Curtis, Doug Pride, Jacob Heck, Kevin Ahlgren, Rick Sauve, Peter Luk, Chris Jekeli, Scott Martin, Jon Wooten, Rob McMillan, James Foster, Ben Brooks, and Abel Brown.

I am sincerely grateful for the unwavering support received from Ross Mackay, Brett Howe, Dan Roman, Dru Smith, and many others at NOAA's National Geodetic Survey, for the ability to do research and pursue this as well as other professional development opportunities.

I would like to acknowledge the inspiring gentlemanly academic competition (a race that I won) with Michael Dennis, who is a true inspiration and friend. He has been a terrific sounding board in keeping up the often-difficult motivation to finish this pursuit, all the while in parallel working full time.

No less deserving of infinite gratitude goes out to my parents (Mom and Dad), Grandma, my Sister and her family, and my extended family, who have always pushed me and provided the best family foundation custom tailored just for me, truly like none other.

A very special thanks to my ever-supporting friends Ken M., Bob C., Dave C., Bill S., Kevin K., Arturo E., Hector P., Juan Carlos B., Brett M., Dave P., Fran C., Brian S., Mario S., Donald T., John M., Chris E., Maria C., and Merle S. for your constant support and contact for all these many years. I am truly fortunate to have such good friends.

A final nod of thanks goes to The Ohio State University's School of Earth Science and the people whom I worked side by side with for more than 10 years. I truly cherish the time spent working with you.

Vita

Degrees and Awards

2013.....D.Sc., [Doctorate of Science, Honoris Causa], Escuela Militar de Ingeniería, La Paz, Bolivia

2013.....M.S., Geodesy/Geophysics, The Ohio State University, Columbus, Ohio

2003.....M.S., Geophysics, University of Hawai'i at Manoa, Honolulu, Hawai'i

1995.....B.S., Earth Science, State University of New York College at Buffalo, Buffalo, New York

1990.....A.S., General Studies, Erie Community College, Buffalo, NY

Additional Academic Preparations

1995-1996 .....Center for the Study of Active Volcanoes, University of Hawai'i – Hilo, Hawai'i

1994.....School of Natural and Built Environments, University of South Australia – Adelaide, Australia

1990-1991 .....Observatorio Vulcanológico, Universidad de Colima - Colima, Mexico

Employment

2014-Present .....Pacific Southwest Regional Advisor (CA, NV), NOAA's National Geodetic Survey (NGS)

2014-Present .....Research Associate, Scripps Institution of Oceanography, IGPP, UCSD

2004-2014 .....Operations Manager - Senior Geodetic Engineer, School of Earth Sciences at The Ohio State University

2002-2004 .....Geodetic Engineer, Sea Level Center at University of Hawai'i

Publications

Bevis, M.; Wahr, J.; Khan, S. A.; Madsen, F. B.; Brown, A.; Willis, M.; Kendrick, E.; Knudsen, P.; Box, J. E.; van Dam, T.; **Caccamise, D. J., II**; Johns, B.; Nylen, T.; Abbott, R.; White, S.; Miner, J.; Forsberg, R.; Zhou, H.; Wang, J.; Wilson, T.; Bromwich, D.; Francis, O. Bedrock displacements in Greenland manifest ice mass variations, climate cycles and climate change Proc. Natl. Acad. Sci. U.S.A., 2012, 109, 11944–11948, doi: 10.1073/pnas.1204664109

Tong, X.; Sandwell, D.; Luttrell, K.; Brooks, B.; Bevis, M.; Shimada, M.; Foster, J.; Smalley, R., Jr.; Parra, H.; Báez, J. C.; Blanco, M.; Kendrick, E.; Genrich, J.; **Caccamise, D. J., II** (2010) The 2010 Maule, Chile Earthquake: Downdip rupture limit revealed by space geodesy, *Geophys. Res. Lett.*, 37, L24311, doi: 10.1029/2010GL045805.

Lee, J. K**.; Caccamise, D. J., II**; Jekeli, C. "The Precise INS/GPS Geolocation of a Vehicle-towed UXO Detection System," *Proceedings of IEEE/ION PLANS 2010*, Indian Wells, CA, May 2010, pp. 1189-1196.

Bevis, M.; Kendrick, E.; Smalley, R., Jr.; Dalziel, I.; **Caccamise, D. J., II**; Taylor, F. W.; Zhou, H.; Brown, A.; Raleigh, D.; Willis, M.; Wilson, T.; Konfal, S. (2009) Geodetic measurements of vertical crustal velocity in West Antarctica and the implications for ice mass balance, *Geochem. Geophys. Geosyst.*, 10, Q10005, doi: 10.1029/2009GC002642.

Bevis, M.; Hudnut, K.; Sanchez, R.; Toth, C.; Grejner-Brzezinska, D.; Kendrick, E.; **Caccamise, D**.; Raleigh, D.; Zhou, H.; Shan, S.; Shindle, W.; Yong, A.; Harvey, J.; Borsa, A.; Ayoub, F.; Elliot, B.; Shrestha, R.; Carter, B.; Sartori, M.; Phillips, D.;

Coloma, F.; Stark, K. (2005) The B4 Project: Scanning the San Andreas and San Jacinto Fault Zones, Eos Trans. AGU, 86 (52), Fall Meet. Suppl., H34B-01.

Caccamise, D. J., II; Merrifield, M. A.; Bevis, M.; Foster, J.; Firing, Y. L.; Schenewerk, M. S.; Taylor, F. W.; Thomas, D. A. (2005) Sea level rise at Honolulu and Hilo, Hawaii: GPS estimates of differential land motion, *Geophys. Res. Lett.*, 32, L03607, doi: 10.1029/2004GL021380.

Caccamise, D. J., II. Sea and Land Level Changes in Hawai'i, Master's Thesis, University of Hawai'i at Manoa, December 2003.

Caccamise, D. J., II; Michaud, J. D. Sub-Grid Variability of Climate-Related Land-Surface Characteristics, NASA Space Grant Fellowship, University of Hawai'i, 1996.

Fields of Study

Major Field: Earth Science

Specialization: Geodetic Science

Table of Contents

List of Tables

List of Figures

Chapter 1. Introduction - Land and sea level changes

1.1 Motivation

Continuous geodetic measurements have been initiated at or near tide gauges in many parts of the world since the late 1990's so that the relative sea level (RSL) histories recorded by these instruments can be transformed into absolute sea level (ASL) histories (Neilan, 1998; Bevis et al., 2002; Caccamise et al., 2005). ASL time series from tide gauges are used to assess temporal drifts in satellite altimeter records (Mitchum, 2000). In addition, global mean sea level reconstruction analyses for time periods before there were satellite altimeters require tide gauge ASL records (Hamlington et al., 2016; Woppelmann and Marcos, 2016). A tide gauge measures RSL, or the height of the sea surface relative to the land or seafloor on which the tide gauge rests. A tide gauge alone cannot distinguish between uplift of the sea surface and subsidence of the underlying seafloor. In contrast, satellite altimeters measure the height of the sea surface relative to a spatial reference frame (RF) such as some variant of the International Terrestrial Reference Frame (ITRF). Repeat altimetry is often described as delivering an *absolute* measurement of sea level change. However, when ASL changes inferred from a tide gauge are compared to ASL changes inferred from one or more satellite altimeters, it is necessary that the satellite orbits and the vertical motions of tide gauges observed by collocated CGPS stations are both expressed in the *same* RF (Bevis et al., 2012). As such

the term absolute is somewhat misleading. It seems to imply a measure that is truly unambiguous, or unique, like the physicist's concept of absolute zero. But actually, what ASL means is sea level expressed in a standard RF. If we change the RF, we will almost certainly change the value of ASL.

The 'CGPS@TG' agenda (Bevis et al., 2002) refers to the use of continuous geodetic GPS (or GNSS) measurements to transform the RSL time series recorded by a tide gauge (TG) into an ASL time series via the relation

$$\Delta ASL = \Delta RSL + VLM \tag{1.1}$$

where ΔASL is the change in ASL, ΔRSL is the change in RSL, and VLM is vertical land motion, i.e. the change in land level, all developed during a common interval of time. Eq. (1.1), which refers to displacements, can be reformulated in displacement rate or velocity space as

$$V_{ASL} = V_{RSL} + V_{LM} \tag{1.2}$$

where V refers to vertical velocity. Space geodesists often use V_U to represent V_{LM}, since U is the up component of motion. If these velocities change over time then this equation applies only to instantaneous velocities (at a common epoch). Eq. (1.1) is valid over extended periods of time even if the rates or velocities are changing, but Eq. (1.2) is not.

When RSL time series obtained from a tide gauge are much longer than crustal displacement time series obtained from a nearby GPS station, a direct application of Eq. (1.1) to vertical displacement time series is restricted to the common time span of observation. This is problematic in that we would like to use the entire RSL time series so as to 'average down' the high noise levels pervading RSL. This can be done if we assume that the velocities in Eq. (1.2) do not change in time, allowing us to combine a VLM rate estimated from a short geodetic time series with an RSL rate estimated from a much longer tide gauge time series. However, assuming constant velocities is rather dangerous, particularly in seismogenic regions, unless some means can be found for accounting for coseismic jumps and postseismic transients affecting both VLM and RSL. Earthquakes aside, one of the main motivations for this entire agenda is to determine if global sea level rise is accelerating, in which case assuming constant velocity is obviously problematic.

1.2 Objectives

In this work we focus on some of the most pressing difficulties of using Eqs. (1.1) or (1.2) to estimate ASL rates at tide gauges: (*a*) the 'contaminating' effect that earthquakes have on VLM and therefore on RSL, and (*b*) the problem of estimating RSL rates using tide gauges that record high amplitude, mostly short-lived sea level fluctuations associated with ocean dynamics. In many regions, especially those subject to strong El Niño events, this 'noise' does not have zero mean value. For example, in the tropical

West Pacific, extreme negative fluctuations in sea-level have larger amplitudes than extreme positive fluctuations. Such skewed noise distributions will usually bias RSL rate estimates obtained from a standard least squares analysis. An additional problem, specific to long time series of RSL, is (c) whether or not we should assume the rate of change of RSL to be constant.

In some areas the two problems identified above can interact, because for time periods in which GPS observations are not available, high amplitude (and temporally correlated) dynamic sea level variations can make it very difficult to determine if RSL time series have been perturbed by seismic activity or not. Therefore our fourth focus, (*d*), is finding ways to reduce ASL noise levels so as to improve our ability to recognize earthquake-related signals in RSL time series when geodetic measurements are not available.

We explore several approaches to (partially) mitigating the large oceanographic fluctuations that dominate ASL and RSL. First, we can try to cancel them out by differencing an altimeter time series (from a point in the ocean close to the tide gauge) and the tide gauge time series. This provides us with a tool that we can use after TOPEX appeared in 1993. Second, we can attempt to reduce the impact of strong El Niño events by incorporating them into the trajectory model using an oceanographic index of some kind. That is, we can try to 'model out' the El Niño events. Lastly, we use a numerical ocean model to estimate the dynamic ocean signal and then remove its influence.

A large fraction of high quality, long-lived tide gauges are located in seismogenic zones, notably along the Pacific coasts of the Americas, across Japan, and at islands along the plate boundaries of the western Pacific. Past estimates of global mean sea level from tide gauges typically omit stations where earthquake related displacements occur in the time series (e.g., Ray and Douglas, 2011). We seek a more nuanced approach where we can still use (some) such time series, but differentiate between the background rate of RSL rise and the perturbations in RSL caused by major earthquakes. These perturbations take the form of coseismic jumps in the vertical position of a tide gauge, and thus in RSL, but large earthquakes also produce sustained transient uplifts. Postseismic transients can persist for a decade or even for several decades (e.g. Wang et al., 2007; Bevis and Brown, 2014). Some tide gauges may be affected by postseismic transients produced by earthquakes that occurred well *before* the tide gauge was established, and these seismic events are easily overlooked. Postseismic transients are non-linear in time, and often violate implicit assumptions that the rate of VLM is constant. However, if we can estimate the jump and the transient explicitly, we retain the option of assuming that the long-term or 'background' rate of sea level change is constant.

1.3 Trajectory Models

We follow Bevis and Brown (2014) in describing the motion of GPS stations using trajectory models. The position vector of a station $\mathbf{x}(t)$ can be decomposed in a geocentric Cartesian axis system{X,Y,Z} or in a local or topocentric Cartesian axis system {E,N,U}

in which the axes point east, north and up. The *standard linear trajectory model* (SLTM) is a kinematic model which is the sum of three displacement modes, or distinct classes of motion, that describe the progressive trend of the trajectory, any instantaneous jumps in position, and periodic or cyclical displacements:

$$\mathbf{x}(t) = \mathbf{x}_{\text{trend}} + \mathbf{x}_{\text{jumps}} + \mathbf{x}_{\text{cycle}} \tag{1.3}$$

Jumps are described as linear combinations of Heaviside jumps at prescribed jump times $\{t_j\}$. The number of jumps, n_J, may be zero, one or more. Jumps include coseismic jumps, which are real movements of the ground, and 'artificial' jumps associated with changes in the GPS antenna and/or its radome, or changes in the antenna monument, etc. Nearly all GPS time series present a seasonal cycle of displacement which can be modelled as a 4-term Fourier series with periodicities of 1 year and 0.5 year. The most common trajectory model invokes a constant velocity trend, in which case the SLTM has the following form:

$$\mathbf{x}(t) = \mathbf{x}_R + \mathbf{v}(t - t_R) + \sum_{j=1}^{n_J} \mathbf{b}_j \, \mathrm{H}(t - t_j) + \sum_{k=1}^{n_F} \left[\mathbf{s}_k \sin(\omega_k t) + \mathbf{c}_k \cos(\omega_k t) \right] \tag{1.4}$$

Where t_R is an arbitrary reference time, often set to the mean time of observation, $\mathbf{x}_\mathrm{R} = \mathbf{x}(t_\mathrm{R})$ is the reference position, and $\mathbf{v}$ is the station velocity vector, which is assumed to be constant. The function H is the Heaviside or unit step function, and vector $\mathbf{b}_j$ describes the direction and magnitude of the jump which occurs at time t_j. The 3-vectors $\mathbf{s}_k$ and $\mathbf{c}_k$

are the Fourier coefficients (one for each component of the position vector) for the harmonic with angular frequency ω_k.

In the event that the station does not move with a constant velocity trend, we can use a more general form of the SLTM in which the trend is polynomial in time, thus:

$$\mathbf{x}(t) = \sum_{i=1}^{n_P+1} \mathbf{p}_i (t - t_R)^{i-1} + \sum_{i=1}^{n_J} \mathbf{b}_j \, \mathrm{H}(t - t_j) + \sum_{k=1}^{n_F} \left[\mathbf{s}_k \sin(\omega_k t) + \mathbf{c}_k \cos(\omega_k t) \right] \tag{1.5}$$

Where n_P is the maximum order of the polynomial. If $n_P = 1$, then this model reduces to the constant velocity model, with $\mathbf{p}_1 = \mathbf{x}_R$ and $\mathbf{p}_2 = \mathbf{v}$. If $n_P = 2$, it becomes the quadratic trend or 'constant acceleration' model in which the acceleration vector $\mathbf{a} = 2\,\mathbf{p}_3$. No matter what the value of n_P, $\mathbf{p}_1$ always corresponds to the reference position $\mathbf{x}_R$. In our experience it is only rarely necessary to set $n_P > 3$. For the large majority of GPS stations, it is adequate to set $n_P = 1$.

The vector equation (1.5) can be thought of as a system of three scalar equations describing the temporal evolution of the X, Y, and Z coordinates respectively. But it can just as easily be used to describe the E, N, and U components of displacement. That is, one could associate $\mathbf{x}_3$ with Z or U.

The SLTM cannot adequately describe postseismic transient displacements. This can be done using exponential or logarithmic transients, and we prefer to use logarithmic

transients. It is well known exponential and logarithmic transients can produce almost identical fits to GPS time series manifesting postseismic deformation, but we have convinced ourselves that logarithmic transients provide very slightly better fits (Sobrero, 2018). A simple logarithmic transient displacement, d, has the form

$$d = A \log(1 + \Delta t/T) \tag{1.6}$$

where A is the amplitude coefficient, T is the characteristic time scale of the transient, and Δt is the time since the earthquake occurred. Since this formula applies only after the earthquake has occurred, we are restricted to the domain $\Delta t > 0$. The scalar d might refer to any one of the geocentric cartesian coordinates (X, Y, or Z) or topocentric Cartesian coordinates (E, N, and U) used to describe a geodetic time series.

Sometimes a significantly better fit to an observed transient can be obtained using a double transient in which there are two characteristic time scales, T_1 and T_2, thus

$$d = A_1 \log(1 + \Delta t/T_1) + A_2 \log(1 + \Delta t/T_2) \tag{1.7}$$

Double transients always provide a better fit than simple transients, since they double the number of adjustable quantities, but they also lead to inversions with considerable larger condition numbers, implying that the solution is less stable and might lead to a less reliable prediction of future behavior despite producing a better fit to the data in hand.

This occurs because the double transient model may start to model the noise as well as the signal. In practice, it is dangerous to invoke double transients if the observations being modeled are highly noisy. As a result, we never invoke double transients where we are modeling tide gauge observations rather than GPS displacements.

We define the *extended trajectory model* (ETM) as the combination of a SLTM and one or more logarithmic transients. Explicitly, the ETM is

$$\mathbf{x}(t) = \sum_{i=1}^{n_P+1} \mathbf{p}_i (t - t_R)^{i-1} + \sum_{j=1}^{n_J} \mathbf{b}_j \, \mathrm{H}(t - t_j) + \sum_{k=1}^{n_F} \left[\mathbf{s}_k \sin(\omega_k t) + \mathbf{c}_k \cos(\omega_k t) \right] + \sum_{i=1}^{n_T} \mathbf{a}_i \log(1 + \Delta t_i / T_i) \tag{1.8}$$

where n_T is the number of logarithmic transients. For each transient caused by an earthquake at time t_{EQ} , we define $\Delta t = 0$ for $t < t_{\mathrm{EQ}}$ and $\Delta t = (t - t_{\mathrm{EQ}})$ otherwise. Note that we can invoke double transients by having the same value of t_{EQ} for two of the Δt_i , but different values for T_i.

In this thesis, we are mostly concerned with vertical land motion (VLM), which is the upwards component of ground displacement, U, or with the vertical motion of the sea surface. Sea level rise can be expressed relative to the land, *i.e.* relative sea level (RSL) change, or relative to an external reference frame, *i.e.* 'absolute' sea level (ASL) change. As a result, we will use the SLTM and the ETM, but only for vertical displacements, and

so the vector equations presented above will normally reduce to scalar equations. The other, less important change is that when we model RSL time series collected by tide gauges, those displacements have already been corrected for tidal displacements. But the tidal models are sometimes imperfect, and so residual oscillations may be present at tidal frequencies. In this case the truncated Fourier series may be augmented to include the major tidal frequencies as well as the annual and semi-annual periodicities associated with seasonal ground motion.

One of the most attractive aspects of the SLTM is that this model is linear in its coefficients, so the task of fitting an observed time series with this model, i.e. solving for the coefficients or parameters of the trajectory model, reduces to solving a linear least squares problem. This is not strictly true for the ETM, but if the characteristic time scales (T) of the logarithmic transients are assigned rather than estimated, then the problem again becomes linear and the ETM is renamed the *extended linear trajectory model* (ELTM). It is often reasonable to pre-assign the transient time scale parameters, particularly when invoking a double logarithmic transient. In this case we usually set T_1= 0.0523 years and T_2 = 1 year, because formally optimizing their values very rarely leads to significant improvements in fit (Wang, 2018). We follow this practice throughout this thesis. When the displacement data are too noisy to justify the use of a double transient, then (provided that there is at least one year of displacement data following the earthquake) we will typically set T = 1 year (Bevis and Brown, 2014).

1.4 Colored noise and confidence intervals

When solving the linear least squares problem, it is conventional practice to compute a covariance matrix for the solution vector, and then use the diagonal of this matrix to form a standard error estimate, σ, for each component of the solution vector (Hamilton, 1964; Menke, 2012). The elements of the solution vector comprise the parameters or coefficients of the model. The *k*, the standard error estimate provides insight into the uncertainty associated with the estimated value of the *k* used in the model parameter. When the noise in the measurements is drawn from a normal distribution *and* is uncorrelated in time, the 95% confidence for the corresponding parameter estimate is 1.96σ, i.e. very close to 2σ. Let *n* be the number of observations in the data or observation vector. As the time series gets longer the value of *n* increases, so, if the amplitude of the noise in the observations is not changing in time (i.e. the process is stationary), the amplitude of the standard error estimate will decline inversely with the square root of *n*. This ensures that the standard errors and the widths of the confidence intervals decline fairly rapidly, if not proportionately, as the length of the time series increases. However, if the noise affecting the observations is correlated in time, and the post-fit residuals are not independent, then dividing by root *n* is problematic because there are not, in fact, *n* independent residuals, nor (*n-m)* residuals where *m* is the length of the solution vector). One can take the point of view that the covariance matrix and therefore the standard errors are defined in a purely geometrical way, and therefore the standard equations used to estimate the standard error estimates are still valid. But if our

definition of the standard error is not modified when the noise is correlated in time, then the 95% confidence interval will not be 2σ, but perhaps $10\,\sigma$ or $30\,\sigma$ instead! Not recognizing that daily coordinate time series for GPS stations are affected by correlated noise, will lead us to seriously underestimate the width of the 95% (or any other) confidence level. That is, we would systematically underestimate the uncertainties attending our parameter estimates.

Noise that is not correlated in time (i.e. from one measurement to the next) is referred to as *white* noise. Its power spectrum is flat, *i.e.* its power spectral density does not vary with frequency. In contrast, power law noise (PLN) has a power spectral density, P, which is a function of frequency, f, with the following form:

$$P(f) = P_o\,(f/f_o)^{\kappa} \tag{1.9}$$

where κ is known as the spectral index of the PLN. Clearly, $P(f_o) = P_o$, and the specific frequency f_o is some (arbitrary) reference frequency. Note that when $\log(P)$ is plotted against $\log(f)$, this curve becomes a straight line with slope κ that passes through point $[\log(f_o), \log(P_o)]$. PLN with $\kappa = -1$ is called flicker noise, pink noise or $1/f$ noise. Note that $1/f$ noise is pronounced "one on f noise". PLN with $\kappa = -2$ is called random walk noise. The designation 'noise' is somewhat subjective, since one scientist's signal can be another scientist's noise. So, it is possible to discuss a process that obeys equation 1.7 for

many decades of frequency, and whereas a geodesist might consider this to be a 'noise process', astronomer or an oceanographer might consider this spectrum to characterize a signal instead. Note that white noise is a special case of PLN for which the spectral index is zero. Be aware that some scientists and engineers define another index $\alpha = -\kappa$, so, for example, flicker noise has $\alpha = +1$. Power law noises with non-zero spectral indices are collectively called *colored* noise. Flicker noise and random walk noise are special cases of colored noise. Although engineers recognize colored noise processes with positive and negative spectral indices, κ, most processes observed in nature have negative values, commonly with $0 > \kappa > -2$. The relative sea level histories recorded by tide gauges often seem to be dominated by power law processes (Agnew, 1992).

Geodesists examining two color geodimeter (distance) measurements and GPS displacements in the 1990s recognized the presence of temporally-correlated or colored noise in their time series (e.g. Johnson and Agnew, 1995; Zhang et al., 1997), and in the next decade many geodesists addressed the problem of producing stochastic models for these noise processes, and figuring out how to adjust or normalize the standard errors they produced for their kinematic models (especially velocity estimates), so that the 95% confidence interval really was very close to $2\sigma^*$ where σ^* is the renormalized, adjusted or 'corrected' value of the conventional standard error estimate, σ. For GPS time series, in particular, it was quickly realized that some combination of PLN and white noise (WN) seemed to be appropriate for most GPS stations, and in many cases a mixture of flicker noise (FN) and WN seemed to account for the residuals about the best fit

trajectory models (Zhang et al., 1997; Mao et al., 1999; Williams, 2003). Various algorithms have been developed for accounting for the impact of colored noise on the confidence intervals of station velocities and other trajectory model parameters (Williams, 2008; Bos et al., 2013), and the OSU geodesy group has implemented a similar algorithm which we use here for computing normalized standard errors, based on the adoption of one of several stochastic noise models: (1) PLN, (2) PLN+WN, (3) FN, or (4) FN+WN. When working with GPS data we have found, as have many other investigators, that PLN+WN and FN+WN seem to work best. For any given station it is very hard to determine which model is best, and we tend to choose the model that produces the more conservative (larger) estimate for the confidence interval.

Suppose we fit a trajectory model to our GPS data and assume (incorrectly) that the measurement noise is white noise (which is uncorrelated in time), and use the classical formulas to compute the standard error estimate, σ, from the post-fit residuals. The conventional assumption that 2σ (truly 1.96σ) constitutes the 95% confidence interval is actually incorrect. Actually the 95% confidence interval is some scale factor f larger than this. If we estimate f by devising a stochastic noise model from the power spectrum of the post-fit residuals, or using another appropriate algorithm, then we could assert that the true 95% confidence interval is $2f\sigma$ (or $1.96f\sigma$ if we are sticklers for detail). The approach more commonly taken in the geodetic community is to report the 'corrected' or normalized standard error estimate $\sigma^* = f\sigma$, and assert that the 95% confidence interval is $2\sigma^*$. We will follow the second approach in this study. However, to simplify our

notation, we will drop the use of σ*, and it should be understood that in all following chapters, we shall use σ for the ‘corrected’ or renormalized standard error.

Chapter 2. Trajectory models for GPS stations in the Samoas

2.1 Location and tectonic setting

There are three long-lived GPS stations in the Samoan archipelago (Fig. 2.1). This group of islands is divided between American Samoa (a territory of the USA) and the independent nation of Samoa, which was called Western Samoa between 1914 and 1997. There are two GPS stations on the island of Upolu in Samoa: one has the station code FALE and is located in the grounds of the international airport, and the other, with station code SAMO, was built in the capital city of Apia. The third GPS station of the archipelago, which has the code ASPA, is located in Tutuila, the main island of American Samoa, in the capital city Pago Pago (which is pronounced Pango Pango).

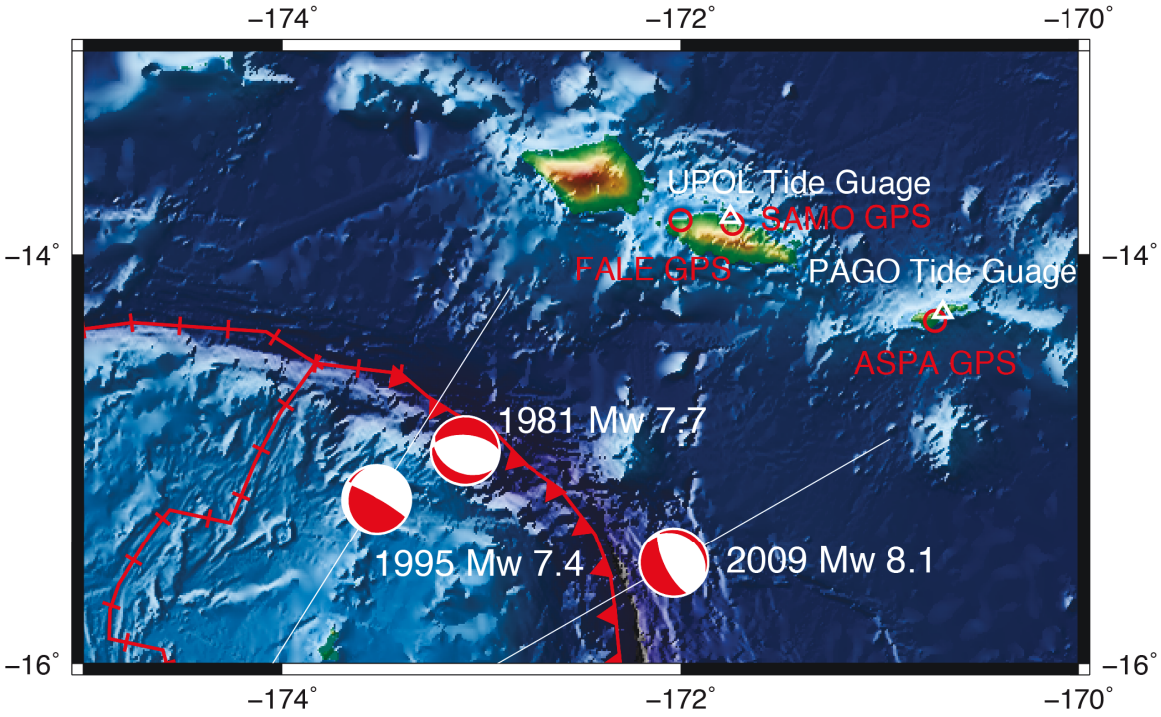

Figure 2.1 Samoa and Pacific region location map. The GPS station ASPA and the tide gauge PAGO are located in the island of Tutuila (American Samoa). The GPS stations SAMO and FALE and tide gauge UPOL are located on the island of Upolu (Samoa).

There are two important tide gauges in the Samoan archipelago. One, built by Australia's National Tidal Facility, is located in Apia harbor on Upolu island. It has tide gauge code UPOL. The other, built by the US government, is located in Pago Pago Harbor, in Tutuila, and has tide gauge code PAGO. The GPS station ASPA is located 6.4 km from the tide gauge PAGO. The GPS stations SAMO and FALE are located 3.8 km and 27 km, respectively, from the tide gauge UPOL. The two tide gauges are 126 km apart. The distances between the GPS stations are FALE-ASPA: 148.4 km, and SAMO-ASPA: 121.7 km and FALE-SAMO: 28.3 km.

GPS station FALE, constructed by M. Bevis in late 1996, incorporates a steel antenna monument coupled directly to bedrock. It is considered a very 'stable' monument in the sense that its movements are those of the underlying lithosphere. Neither SAMO or ASPA are built into bedrock.

All of the Samoan islands lie within the Pacific plate, close to a subduction zone associated with the Tonga trench and island arc (Bevis et al., 1995). The Tongan island arc is separated from the Australian plate by the Lau Basin, an active back-arc basin. The subduction rates at the Tongan trench increase northwards, reaching a maximum value of ~ 250 mm/yr near the northern terminus of the trench. Most plate convergence at the subduction zone is aseismic, but there are some large seismic events. Large, shallow earthquakes with epicenters in or close to the Tonga trench tend to be of three kinds: low dip angle underthrusting earthquakes on the plate interface or megathrust; normal faulting earthquakes in the outer trench wall or outer rise; and "hinge-faulting" or "trap-door" events, close to the northern limit of the Tonga trench, where the subducting portion of the Pacific plate to the south has to detach (by tearing) from the adjoining part of the Pacific plate, to the north, which does not subduct. The major historical earthquakes in the general region of the Samoan islands are listed in Table 2.1.

Table 2.1 The major historical earthquakes near the Samoan Archipelago.

Location		Moment Magnitude	Distance from PAGO	Date of E.Q.	E.Q. S - score
Latitude	Longitude	(Mw)	(km)	yyyy-mm-dd	>.2 is Sig.
-14.739	-173.562	8	313.998	1917-06-26	0.425413
-18.352	-172.515	8.1	492.82	1919-04-30	0.303777
-16.264	-172.467	7.8	291.738	1975-12-26	0.355229
-16.696	-172.095	7.6	307.982	1977-04-02	0.236696
-14.96	-173.085	7.7	269.137	1981-09-01	0.336746
-15.199	-173.529	7.4	322.502	1995-04-07	0.121236
-20.187	-174.123	8	751.154	2006-05-03	0.0952108
-15.489	-172.095	8.1	202.454	2009-09-29	0.640569

The S score listed in Table 2.1 is an empirical statistic developed at OSU that predicts the likelihood of an earthquake causing a significant jump and/or transient at a specific point or station, based on the distance between the earthquake and the station, and the magnitude of the earthquake. S values near zero, or less than zero, are very unlikely to cause significant displacements, and S values > 0.2 are very likely to produce significant displacements. Seismic events producing S values at or above 0.5, for example, *always* produce very large jumps and transients. This statistic, which was developed by an analysis of a very large, globally distributed set of GPS stations from 1994 to present, and the USGS earthquake catalog, suggests that for stations in the vicinity of Pago Pago, the 2009 earthquake very likely produced the largest coseismic and postseismic displacements of any seismic event since 1917.

The 29 September 2009 seismic event was by far the most important event that has occurred in the lifetime of all three Samoan GPS stations. It was also a very unusual

'composite' event – i.e. a pair of coupled, nearly simultaneous earthquakes (Beavan et al., 2010). One event occurred on the subduction interface and the other occurred in the outer-rise on the opposite side of the trench axis. Both events had moment magnitudes $M_w \sim 8$, but they are often listed in earthquake catalogs as a single event of magnitude 8.1, because they are very difficult to separate. In the rest of this thesis we will treat them as a single event.

The almost instantaneous coseismic jumps produced by an individual earthquake, and the much more protracted postseismic transient motions, tend to diminish with increasing distance from the center of the earthquake rupture zone, as well as with azimuth. GPS station ASPA was located 196 km from the nominal center (15.49° S, 172.09° W) of the Mw 8.1 doublet, whereas GPS stations FALE and SAMO were only 184 km and 186 km distant, respectively. These distances are fairly similar. However, viewed from the centroid of the earthquake, ASPA has an azimuth much closer to the azimuth of the seismic slip vector than do either FALE or SAMO, so one would expect the largest displacements at ASPA. The azimuth of FALE is more removed from the azimuth of the slip vector, than is the case for SAMO, so one would expect the displacements at SAMO to be larger than those at FALE, but smaller than those at ASPA.

2.2 Trajectory models for GPS stations FALE, SAMO and ASPA

Here we present the vertical displacement time series from OSU's global GPS solution g08b which is expressed in the reference frame OSU2008 which is OSU's realization of the International Terrestrial Reference System, realization 2008 (ITRF2008). In Fig. 2.2, the daily GPS solutions are shown as blue dots, and the best fit trajectory models as red lines. The ELTM trajectory models invoked a double logarithmic transient with timescales of 0.0523 years and 1.000 year. Note that 0.0523 years is the logarithmic mean of 1 day and 1 year.

The weighted root mean squares (WRMS) vertical scatters of the daily GPS positions about the trajectory models are SAMO: 8.5 mm, FALE: 8.4 mm and ASPA: 9.1 mm. These WRMS values are slightly higher than the typical scatter levels observed worldwide (4 - 6 mm), mostly due to the extreme humidity in the tropical West Pacific. Water vapor fluctuations are the single largest cause of positioning error in most of the world. Note that vertical daily scatter levels are roughly 3 times larger than horizontal scatter levels, which is fairly typical of the global pattern.

The level of vertical positioning noise at the three GPS stations is very small compared to the variability of daily RSL levels recorded by tide gauges, even after the ocean tides have been removed.

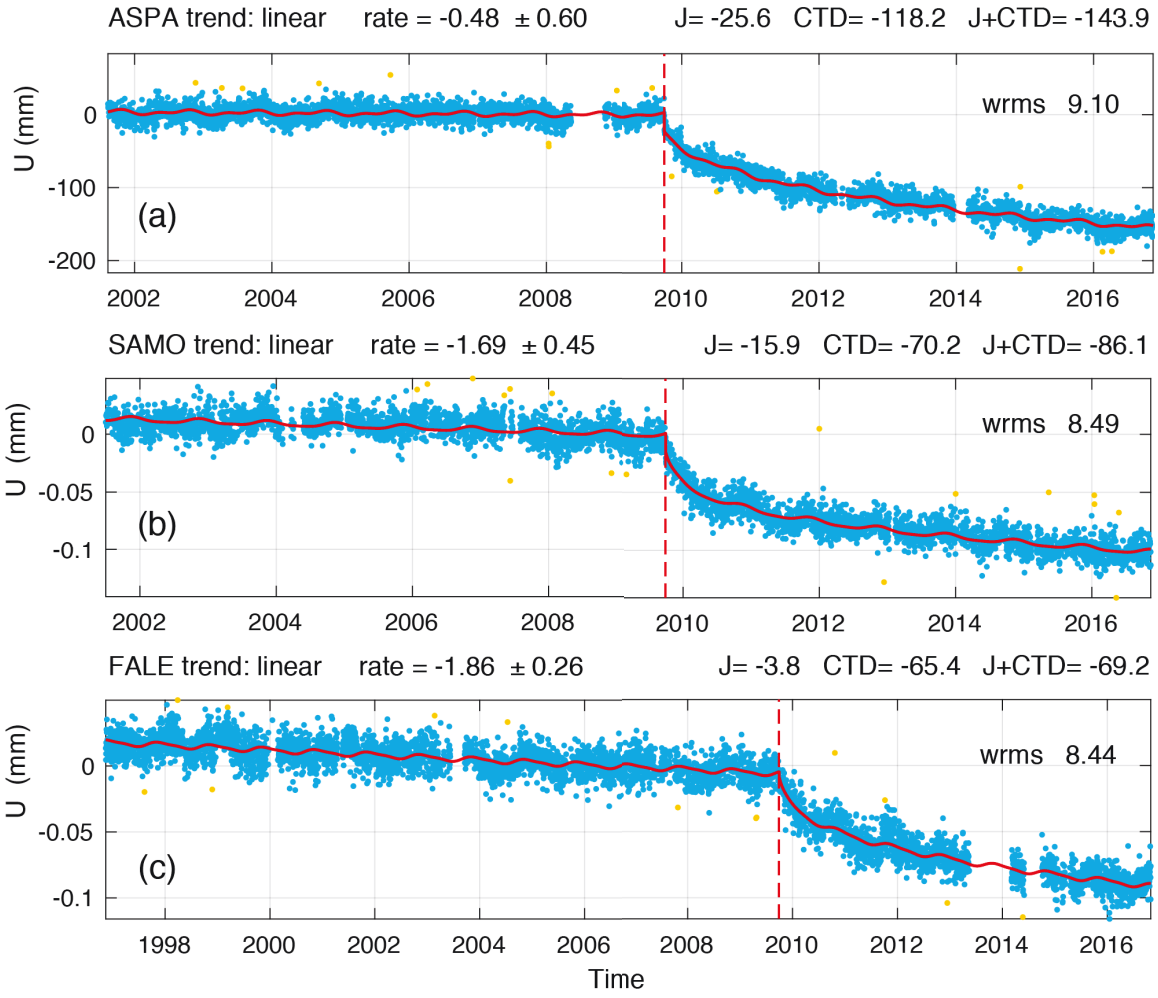

Figure 2.2 The daily GPS time series for the up (U) component of motion, and the ELTMs, for ASPA, SAMO and FALE. Above each plot we list the rate (mm/yr), the jump amplitude, J, the cumulative transient displacement, CTD, at epoch 2015.8, and J+CDT, all in mm.

Above each of the subplots in Fig. 2.2 we list the trend rate (i.e. the velocity, V_U or V_{LM}) in mm/yr, the amplitude of the coseismic jump (J), the cumulative transient displacement (CTD) at the epoch 2015.80, and the sum J+CTD, which is the total seismic perturbation at epoch 2015.8, all in mm. We adopt the reference epoch 2015.8 because it is the end date for our tide gauge time series, so this epoch can be used with all of our time series. Note that the coseismic and postseismic displacements diminish in moving from ASPA to

SAMO to FALE, much as one would expect based on the focal mechanism of the 2009 earthquake (Fig. 2.1).

We list in Table 2.2 these velocity solutions and their renormalized standard errors, based on the noise model adopted (Chapter 1). During the rest of this thesis we will adopt the error estimate associated with the flicker noise plus white noise model (FNWN), because (i) this is the most conservative assumption we can make, and (ii) this is the model preferred by most GPS geodesists for the colored noise at most stations. The FNWN model produces standard error estimates that are 6.2 – 7.1 times larger than the naïve or 'conventional' estimates for standard error that are valid only for pure white noise (i.e. positioning noise that is uncorrelated in time). We note that this pure white noise assumption is often unstated or implicit, and almost always unjustifiable. However, while it is better to estimate standard errors for the trajectory model parameters using a colored noise model, it is not that easy to justify the 'best' choice of model even when we are talking of a large suite of GPS stations. It is even harder to do so for any single station, as can be seen in Fig 2.3, where we show the empirical power spectrum of the post-fit residuals at ASPA and the best fitting stochastic noise model. Clearly the FNWN and the PLNWN models seem to fit the spectrum rather better and does the PLN model. But one cannot make a really compelling argument that the FNWN model is 'better' than the PLNWN model, or vice-versa.

Table 2.2 Some key trajectory model parameters for GPS stations FALE, SAMO and ASPA. Vu is the vertical velocity component of displacement. The standard error estimate for Vu depends on the stochastic noise model we adopt for positioning error. Jump refers to the vertical coseismic jump produced by the 2009 earthquake. The amplitude parameters for the double logarithmic transient are A1 and A2. We also compute the cumulative transient displacement (CTD) at epoch 2015.8 (about 3 months after the last epoch for our tide gauge time series), which is 6.06 years after the earthquake. This is the net effect of the transients developing with time scale parameters T1 and T2.

GPS station code	*Vu* (mm/yr)	Standard error for the vertical velocity (Vu) depending on the choice of noise model (mm/yr)			Jump (mm)	A_1 (mm)	A_2 (mm)	CTD at 2015.8 (mm)
		FNWN	PLNWN	PLN				
FALE	-1.861	0.26	0.20	0.11	-3.8	-10.0	-9.0	-65.4
SAMO	-1.694	0.45	0.37	0.21	-15.9	-13.4	-3.2	-70.2
ASPA	-0.481	0.59	0.49	0.28	-25.7	-5.9	-46.1	-118.2

The standard errors for the rate estimates shown in Fig. 2.2 are those for the flicker noise plus white noise (FNWN) model which we slightly prefer over the power law noise plus white noise (PLNWN) model and greatly prefer over the power law noise (PLN) model.

It is difficult to interpret the amplitude coefficients for the double logarithmic transient since their relative contribution to the combined multi-scale transient depends on the time that has elapsed since the earthquake occurred. This is why we evaluated the total transient displacement that had developed by epoch 2015.8. Note that this

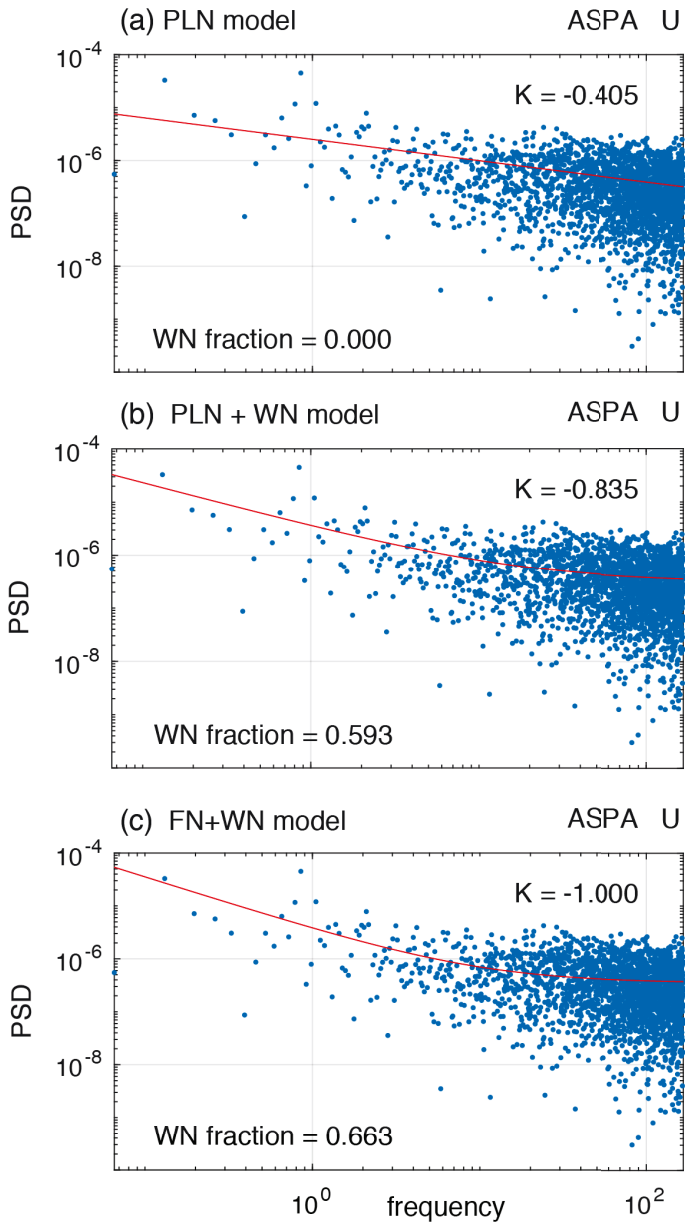

Figure 2.3 The power spectra and competing noise models for GPS ASPA

displacement, which accumulated over the ~6 year period following the earthquake, is much larger than the (effectively instantaneous) coseismic jumps that occurred during the earthquake. The total seismic perturbation at 2015.8 is found by adding the jump (J) to

the cumulative transient displacement (CTD). It is this combination, (J+CTD), that will be sensed most strongly by tide gauges, though its impact on RSL will involve a change in sign: when the ground displaces downwards, RSL rises by an equal but opposite amount. RSL time series are so 'noisy' that it is very difficult for them to sense small coseismic jumps such as those recorded by FALE, but since the cumulative transients grow over time, the combined seismic perturbation J+CTD will eventually become quite apparent.

It is of interest to determine if the differential or relative rate of uplift between FALE and SAMO are significantly different: they are located on the same island, and the distance between them is modest compared to the distance to the 2009 earthquake. Suppose the uplift rate at station A is $r_A \quad \sigma_A$ while that at station B is $r_B \quad \sigma_B$. Suppose we define the differential rate as $\Delta r = r_A - r_B$ then the standard error on this quantity, σ_Δ, is of interest because it will tell us whether or not Δr is significantly different from zero. If the measurement errors at A are independent of the measurement errors at B, then

$$\sigma_\Delta^2 = \sigma_A^2 + \sigma_B^2 \tag{3.1}$$

We do not want to use the conventional standard error estimate based on the assumption of white noise, or uncorrelated errors, because we understand that this will lead to unjustifiably optimistic estimates of uncertainty. But the values of the normalized or corrected standard errors (chapter 1, section 4) depend on the stochastic noise model that

we adopt for GPS positioning noise (Table 2.2). We propagate the errors for each of the noise models in turn and present them in Table 2.3, where we also address whether or not $\Delta r \quad \sigma_\Delta$ is significantly different from zero at the 95% confidence level. In the case of FALE and SAMO, the differential vertical velocity is not significantly different from zero no matter which noise model we adopt. But this is not true for the differential uplift of ASPA with respect to SAMO. This difference is not significantly different from zero only if we adopt the FNWN model, which yields the most conservative standard error estimates. If we adopt the PLN model, which produces the smallest error estimates, then the differential velocity is significantly different from zero. Indeed, if we adopt the PLNWN model, which delivers error estimates of intermediate magnitudes, then we find we are essentially on the boundary between significantly different and not significantly different.

Table 2.3 The uncertainty on the differential uplift rates between FALE and SAMO (same island) and ASPA and SAMO (different islands), and whether or not the differential rate is significantly different from zero, depending on the stochastic noise model adopted for GPS positioning error. All quantities have units of mm/yr

Stochastic Noise Model	$\Delta r = r_{FALE} - r_{SAMo}$			$\Delta r = r_{ASPA} - r_{SAMO}$		
	Δr	σ_Δ	Sig. Diff.?	Δr	σ_Δ	Sig. Diff.?
FNWN	-0.17	0.52	no	+1.23	0.74	no
PLNWN	-0.17	0.42	no	+1.23	0.62	marginal
PLN	-0.17	0.24	no	+1.23	0.35	yes

The fact that the geodetic estimates for the rate of vertical displacement at FALE and SAMO are not significantly different increases our confidence in the stability of the monument at SAMO. We know that FALE is stable in the engineering sense, since it is built into bedrock. All indications are that SAMO has a stable monument as well. Of course, this does not tell us if the tide gauge UPOL close to SAMO is stable. The question of whether or not there is relative vertical motion between a tide gauge and some nearby GPS reference station is always of concern (Bevis et al., 2002), and relative motion can arise if there is engineering instability at either end of the baseline.

Chapter 3. An introduction to satellite altimetry and "ALT-TG"

3.1 Satellite Altimetry

The most celebrated of all satellite altimetry missions was TOPEX/Poseidon, the first satellite altimeter to have a very well constrained orbit. Since then there have been other successful satellite altimetry missions. NASA's TOPEX mission is divided into two sub-missions (TOPEX A and B) because of equipment degradation problems that required a change in operational procedures, and ultimately a change to the redundant backup input altimeter, in order to maintain system performance. TOPEX was eventually replaced by the NASA-CNES missions JASON-1 and JASON-2 (Macmillan et al., 2004) and finally by JASON-3. Several groups have attempted to adjust the results obtained by TOPEX - Jason-2 into a single seamless solution that represents the temporal history of ASL from 1993.6 to 2015.8, or beyond, on a grid of reference points that cover most of the oceans. Forming multi-altimeter solutions for ASL is technically difficult because (1) altimetry collected over long periods of time must be corrected for possible instrument drift using tide gauges, and those tide gauges record land motion as well as changes in sea level, and (2) the measurements of sea level produced using the various altimeters are expressed in the spatial reference frames (RFs) used by geodesists to compute the orbital solutions for those satellites, and even when the geodesists agree in principle on the definition of a common RF spanning the entire time period, it is difficult to realize these frames in a

completely consistent manner. This problem is known as reference frame realization error (Dietrich et al., 2001; Bevis and Brown, 2014). Nevertheless, multi-mission altimeter solutions are certainly good enough to monitor the high-amplitude, dynamic fluctuations in sea level associated with the shifting patterns of the global wind field, and with air-sea interactions such as the El Niño – Southern Oscillation (ENSO) phenomenon. But it is much more challenging to reduce the levels of error affecting multi-altimeter solutions to the point that they can be used to study low-amplitude, slowly developing changes in global mean sea-level (GMSL), and even inquire into the rate of acceleration of GMSL rise (Watson et al., 2015; Nerem et al., 2018).

Table 3.1 The time windows of the four altimetry missions (TOPEX A and B, JASON-1 and JASON-2) used to form the multi-mission altimetry solution used in this thesis.

Altimeter Mission	Mission start	Mission end	Data Start Date	Data End Date
TOPEX-A	08/1992	02/1999	1993.16	1999.11
TOPEX-B	02/1999	10/2005	1999.11	2002.37
JASON-1	01/2002	02/2009	2002.37	2008.53
JASON-2	06/2008	On-going	2008.53	2015.40

The need to improve our understanding of the RSL changes recorded by tide gauges, in order that these time series can be used to improve the calibration of satellite altimetry, is one of the main motivations of this thesis research. But for the present chapter we reverse the logic, and simply adopt the multi-mission altimeter solution of (Beckley et al., 2016) for the space-time variability of ASL, and see what it can tell us about vertical land

motion at tide gauges. Towards the end of this study, we will briefly address the accuracy of the multi-mission altimeter solutions.

3.2 Estimating vertical land motion (VLM) using altimetry and tide gauges

If we recall equations 1.1 and 1.2 from Chapter 1 of this thesis, we can see that it is possible to reverse the logic that motivates our study, and attempt to estimate vertical land motion by subtracting RSL recorded by a tide gauge from what is nominally an ASL time series produced by one or more satellite altimeter missions. That is, VLM = ASL – RSL. Since the ASL time series is derived from altimetry, and RSL time series are derived from tide gauges (TGs), this combination is often referred to as "ALT-TG", for short.

It seems rather odd to estimate VLM using VLM= ALT-TG, since it would normally be easier and far more accurate to estimate VLM using geodetic GPS observations. But there are at least two possible applications that motivate study of the combination ALT-TG.

The time series ALT-TG has far less oceanographic 'noise' than does RSL recorded by a tide gauge. This 'noise' can also be considered to constitute a signal, i.e. dynamic variations in sea surface height (SSH) driven by the global wind field, and air-sea interactions such as the El Niño - La Niña phenomenon. Many scientists interested in global warming and long-term sea level rise are not interested in dynamic SSH variations.

SSH variability is also viewed as noise by geodesists who are worried about whether or not the RSL time series recorded by a given tide gauge has been perturbed or 'contaminated' by earthquakes. This brings us to the first application of the ALT-TG combination: searching for relatively subtle seismic perturbations in the RSL time series produced by tide gauges.

Figure 3.1 shows the vertical displacement time series recorded by GPS station ASPA (Fig. 3.1a), the RSL time series recorded by the nearby tide gauge PAGO (Fig. 3.1b), and the combination ALT-TG formed by subtracting the RSL time series from the multi-altimeter ASL time series for a nearby reference point in the sea offshore from PAGO (these points are about 10 km apart). We fit each of these time series with an ELTM. Let's not worry about the details right now, but focus instead on the following:
a) As expected, ALT-TG does mimic the pattern of vertical land motion recorded by ASPA, and the seismic perturbation produced by the 29 September 2009 earthquake has the opposite sign in the RSL time series
b) the WRMS scatter levels about the ELTM are about 9 mm for the GPS time series, 67 mm for the tide gauge time series, and 26 mm for ALT-TG.

The post-fit scatter of RSL recorded by the tide gauge is 7.4 times larger than the scatter levels in the GPS time series, and 2.6 times larger than the scatter levels in ALT-TG. If an oceanographer looking at the PAGO RSL time series did not know about the 2009 earthquake, he or she might take some time to notice the upwards perturbation caused by

the earthquake. If the perturbation was half as big, it might *never* be noticed! It would be hard not to notice the seismic perturbation in the ALT-TG at first glance, even if the amplitude was halved. This establishes one important application of ALT-TG time series: they are better suited to detecting modest seismic perturbations than are the raw RSL time series. We can use ALT-TG to search for seismic perturbations at tide gauges that do not have a nearby GPS station, and to look for earthquakes in the time period after TOPEX was launched but before any nearby GPS station was constructed.

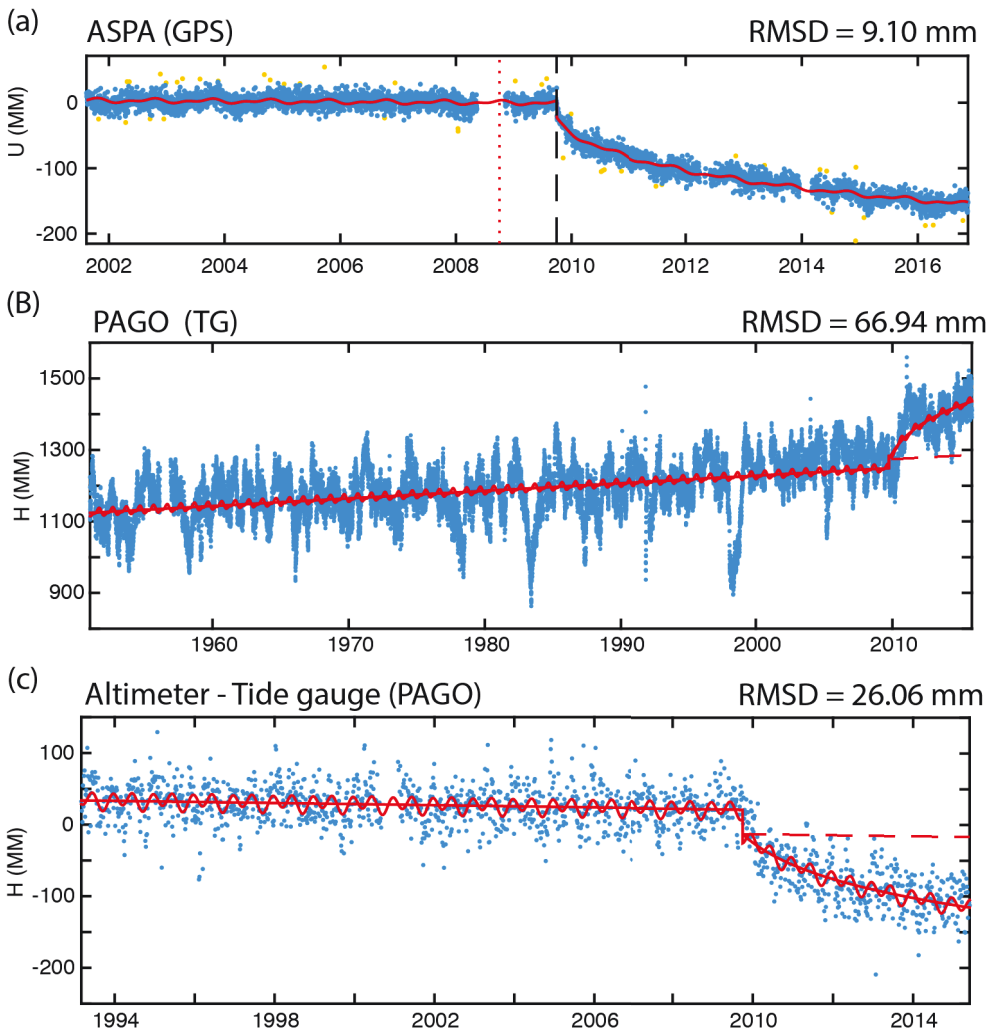

Figure 3.1 Vertical displacement time series in American Samoa. The time series recorded by GPS station ASPA (Fig. 3.1a), the RSL time series recorded by tide gauge PAGO (Fig. 3.1b), and (Fig.3.1c) the combination ALT-TG formed by subtracting the RSL time series from the multi-altimeter ASL time series. All three time series have been fit with an ELTM in order to assess the level of scatter about the trajectory model.

This example motivates us to search for other ways to suppress the high scatter levels in raw RSL time series. We return to this topic in the next chapter.

Fig. 3.1 does establish that ALT-TG is reproducing VLM with some degree of fidelity, certainly with enough precision to establish that the only earthquake that has produced really significant ground motion near PAGO after 1993 was the 2009 event. But this does not mean that ALT-TG can play a significant role in the central task of the CGPS@TG agenda, converting RSL to ASL. That is, we cannot reasonably use a VLM rate inferred from ALT-TG to 'correct' an RSL rate inferred from a tide gauge so as to estimate the ASL rate at that same gauge. This would amount to a tautology, "building in" the conclusion that the ASL rate at the gauge = RSL rate - (ALT-TG) rate = RSL rate – (ASL rate from altimetry – RSL rate) = ASL rate from altimetry. This circular logic does not constitute a valid approach when the goal is to calibrate the altimeter.

In principle, at least, ALT-TG might be used in a different context: to help us assess whether or not the spatial RF used to estimate ASL using one or more altimeters is actually (not just nominally) equivalent to the RF (used by other geodesists) to compute VLM rates for GPS stations located close to our tide gauges. Suppose for example, that the GPS geodesists' frame was translating along the Z-axis (i.e. northwards) relative to the altimetry frame. Then the difference in the VLM rates inferred from GPS and ALT-TG for a global set of tide gauges ought to vary systematically as a function of their latitude, producing increasing positive biases in one hemisphere and increasing negative biases in the other, as the distance from the equator increased. However, this approach to finding relative frame drift will be practical only if the accuracy of VLM determination from ALT-TG is comparable to that obtainable using GPS.

There are many reasons why this might not be the case. For example, the combination ALT-TG does not involve subtracting RSL from ASL at the same point. The nearest spatial grid point for the multi-mission altimeter solution might be 5-10 km distant from the tide gauge. If the sea surface has been tilting rather than just rising, the differential rate of sea level rise between the altimeter reference point and the tide gauge would be injected into the estimate for VLM. This is not an abstract concern, because Caccamise et al. (2005) have already demonstrated such sea surface tilting (i.e. laterally changing rates of ASL) in Hawaii. Another concern, which we will address in a later chapter, is how can we be sure that no inter-mission biases in ASL rate were introduced or admitted when the results from the four altimeters were adjusted into a single, global solution for ASL history? Biases of order 1 mm in space, and 0.5 mm/yr in rate, might not degrade the value of this solution for studying high amplitude, dynamic phenomena such as the El Niño, or regional wind field stressing of the sea surface, but they could be quite problematic for studies of global mean sea level (GMSL) rise, particularly if those biases slowly shift in space and time.

3.3 Estimating VLM rates at tide gauges PAGO and UPOL using ALT-TG

Having established the value of the ALT-TG combination for assessing displacements of the ground at a tide gauge when they are > 1 cm, and having acknowledged concerns about small biases or systematic errors that might attend rate estimates, we now turn to the problem of quantifying the rate of steady vertical displacement and the amplitudes of

the displacement perturbations imposed by the 2009 earthquake, using ALT-TG. These results are shown for tide gauge PAGO in Fig. 3.2a and Table 3.2 and for tide gauge UPOL in Fig. 3.2b and Table 3.3. In the tables, the ALT-TG estimates for land motion are compared with those obtained at the nearest GPS station.

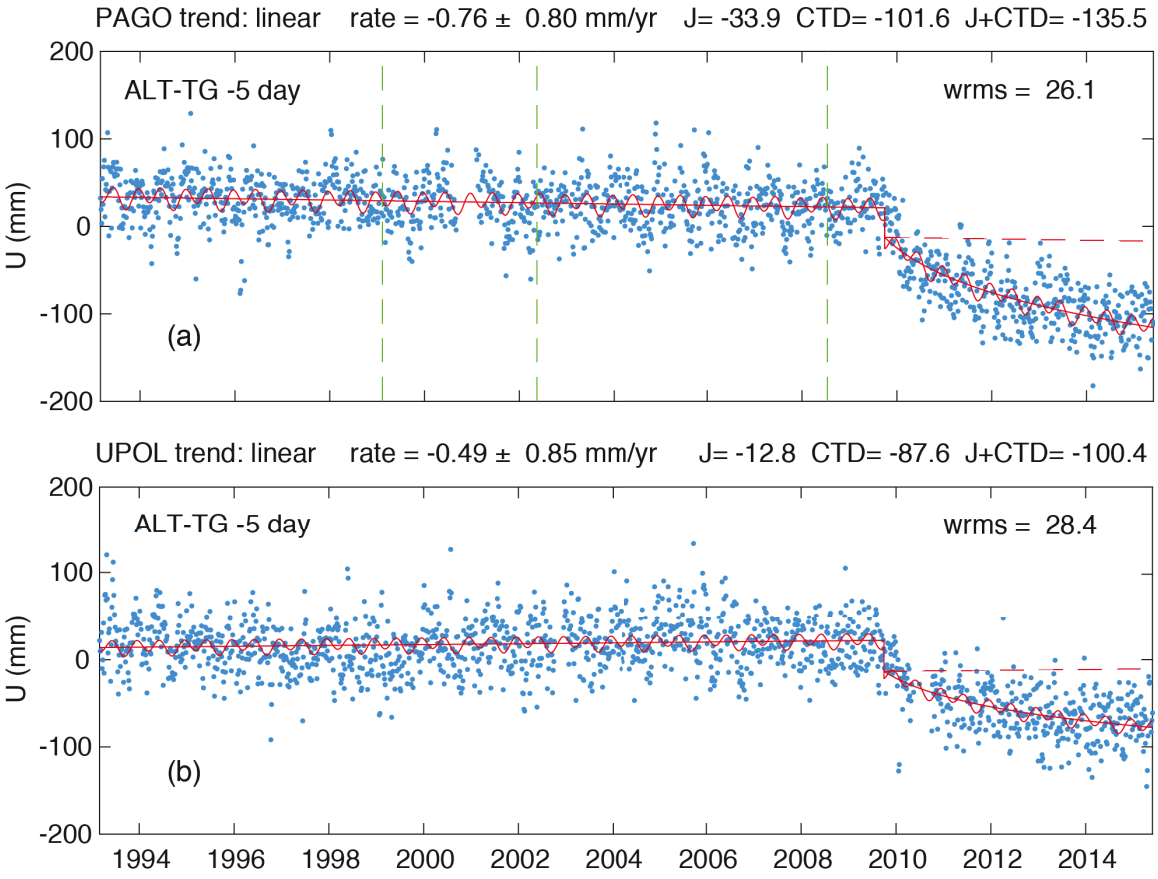

Figure 3.2 The ALT-TG combination that nominally constitutes vertical land motion, for the tide gauges (a) PAGO (American Samoa) and (b) UPOL (Samoa), and their best fitting ELTMs. Above each subplot we list the rate (mm/yr), the jump amplitude, J, the cumulative transient displacement, CTD, at epoch 2015.8, and J+CDT, all in mm.

In order to compare the vertical displacement rates at a tide gauge and a nearby GPS station in a meaningful way, there is an important complication that has concerned both oceanographers and geodesists for many years. Many tide gauges are constructed on harbor walls or piers built on engineering fill, and therefore there may be local subsidence of the structure supporting the tide gauge as the fill compacts under the weight of the structure. The GPS station is presumed to measure the vertical motion of the Earth's crust or lithosphere at the GPS station. But any local, near-surface subsidence (i.e. 'engineering instability') of the tide gauge would be superimposed on crustal motion. This is a straightforward correction given a geodetic estimate of subsidence rate. Concerns about tide gauge stability have caused oceanographers to build, observe and re-observe leveling networks for this purpose (Bevis et al., 2002). There is very little subsidence affecting the tide gage PAGO. But the harbor wall in Apia is large and heavy, relatively young, and built on thick engineering fill. A regular program of 1st order leveling performed by Australian surveyors over many years indicates that the wall supporting the tide gauge is subsiding at 0.82 mm/yr. This requires a major correction for the vertical velocity or rate estimates obtained from ALT-TG, and also for the transient deformation, since this develops over many years. Therefore, it is necessary to compare the GPS trajectory parameters with the corrected ALT-TG trajectory parameters in the right-hand column of each table.

Table 3.2 The rates of vertical motion at Tutuila, the coseismic jump (J), the cumulative transient displacement at 2015.8 (CTD) and J+CDT inferred from the GPS station ASPA, and (via ALT-TG) for the tide gauge PAGO. The results for PAGO are corrected for local, shallow subsidence of the structure supporting the tide gauge (last column). Rates and 1-sigma standard errors are given in mm/yr.

Pago Pago, Tutuila Island, American Samoa				
	ASPA GPS	PAGO ALT-TG	Pier motion (leveling)	Pago Pago crust $(ALT\text{-}TG)_{CORR}$
Rate (mm/yr)	-0.48 0.60	-0.76 0.48	-0.03 0.26	-0.73 0.55
Jump, J (mm)	-25.6 6.2	-33.9 3.7		
CTD (mm)	-118.2 7.1	-101.6 5.1		-101.4 5.3
J+CTD (mm)	-143.9 5.6	-135.5 3.2		-135.5 6.5

We can see that there is no statistically significant difference between the vertical crustal velocities (VLM rates) inferred from the ASPA GPS station and using ALT-TG at the PAGO tide gauge. The amplitudes of the coseismic jumps, the cumulative transient displacement at our reference epoch 2015.8, and the sum of the jump and the cumulative transient are also statistically indistinguishable for the Pago Pago stations. Note that the standard error for the combined jump and transient (J+CTD) is smaller than those for the jump (J) or the cumulative transient displacement (CTD) at 2015.8. This is because the covariance matrix for the trajectory model parameters reveals that the errors affecting (or uncertainties attending) J and CTD are strongly anti-correlated.

Table 3.3 The rates of vertical motion at Upolu, the coseismic jump (J), the cumulative transient displacement at 2015.8 (CTD) and J+CDT inferred from the GPS station SAMO, and (via ALT-TG) for the tide gauge UPOL. The results for PAGO are corrected for local, shallow subsidence of the structure supporting the tide gauge (last column). Rates and 1-sigma standard errors are given in mm/yr.

Apia, Upolu Island, Samoa				
	SAMO GPS	UPOL ALT-TG	Pier motion (leveling)	Apia crust $(ALT\text{-}TG)_{CORR}$
Rate (mm/yr)	-1.69 0.45	+0.48 0.51	-0.82 0.15	+1.30 0.53
Jump, J (mm)	-15.9 6.3	-12.8 6.0		
CTD (mm)	-70.2 7.1	-87.6 7.4		-82.6 7.5
J+CTD (mm)	-86.1 5.3	-100.4 3.2		-95.4 9.0

In contrast, the results obtained for the VLM rates at SAMO and UPOL are statistically incompatible (-1.69 0.45 mm/yr versus +1.30 0.53 mm/yr) at the 95% confidence level once the local subsidence correction has been made. It is not possible to explain this in terms of a relative drift between the GPS and the altimetry reference frames, since any such frame drift would produce essentially similar artifacts in Pago Pago and Apia. Furthermore, we cannot explain the difference in VLM rates between SAMO and UPOL, i.e. 2.99 0.70 mm/yr, by claiming the GPS station is affected by local vertical instability of this amplitude, because we have already seen in Chapter 2, that the vertical velocities of SAMO and FALE are in excellent agreement, and FALE is coupled directly to bedrock.

However, the results for the jumps and the transients at SAMO and UPOL are statistically compatible once the local subsidence correction has been made. We conclude that ALT-TG is useful for estimating seismic perturbations with amplitudes much larger

than 1 cm, but is not sufficiently precise (or stable) for inferring VLM rates of order 1 mm/yr.

The main value of the combination ALT-TG, in our opinion, is as a diagnostic tool for assessing the quality of RSL time series, and especially for detecting previously unsuspected seismic perturbations in RSL time series, when there is no nearby GPS station available to do this more directly.

In the next chapter we turn to the problem of accurately estimating the long-term rate of RSL rise at tide gauges in the presence of the high amplitude, temporally-correlated noise clearly visible in Fig. 3.1b. We cannot use ALT-TG to help us assess RSL rate, other than helping us search for seismic perturbations in RSL time series. But we can mitigate the impact of dynamic sea surface height (SSH) variations by other means. These approaches were in some sense motivated by our ability to suppress SSH variations in ALT-TG. This noise suppression works because much of the SSH variability in the altimetry and in the tide gauge observations is 'common mode' (at least for nearby points), so that it cancels out when these time series are subtracted.

3.4 Using ALT-TG to probe the consistency of the multi-altimeter ASL solutions

Given that the combination ALT-TG eliminates a large fraction of dynamic SSH variability, it should enable us to assess the consistency of multi-mission ASL solutions because small inconsistencies in ASL or ASL rate from one mission to the next will be easier to recognize when they are not buried in high amplitude SSH 'noise'. We can do this by examining ALT-TG time series obtained for various tide gauges and marking on these plots the time of change-over from one altimeter to the next. Fig. 3.4 combines ALT-TG time series for the following tide gauges: Astoria, US (ASTO), Broome, Australia (BROM), Ceuta, Spain (CEUT), Honolulu (HONO), Kwajalein (KWAJ), Lamu, Kenya (LAMU) and Lord Howe Island (LHIS). There are some striking discontinuities in state (sea level) and/or rate. The most obvious discontinuity is that between the Jason-1 and Jason-2 time periods at LHIS. This is a discontinuity in state and rate. There is an apparent discontinuity in rate, but not in state, at the TOPEX-A to TOPEX-B transition in the ASTO time series. The TOPEX-B solution for HONO seems to have a different rate from the TOPEX-A and Jason-1 solutions, and there is a state discontinuity at the TOPEX-A to TOPEX-B transient, but not between TOPEX-B and Jason-1.

Adjusting multiple altimeter solutions into a single and completely seamless solution would be possible only if the four solutions were completely compatible. The existence of the mission-boundary artifacts suggest that the independent solutions were not quite

consistent with each other. These small artifacts would not be visible in the ASL solutions because they would be buried in far larger oceanographic signals. If an oceanographer is concerned with tracking an El Niño event producing decimeter changes in sea level, these subtle inconsistences will do very little damage. But this level of inconsistency is of greater concern if one is attempting to study spatial variations in the rate of ASL rise, or seeking to identify decadal accelerations in ASL rate which have a magnitude smaller than 1 mm/yr/decade.

The main focuses of this thesis are the problems of analyzing tide gauge RSL time series so as to estimate RSL rate, using GPS time series to convert RSL rate to ASL rate, and finally to figure out a methodology for working with tide gauges in which RSL has been perturbed by coseismic and postseismic displacements of the ground. Our overall motivation is helping the oceanographers to calibrate their altimeters using tide gauge data. That is, our position in the overall workflow is near the front end of the process: altimeter calibration. It is not our function to identify or diagnose problems in already existing altimeter solutions. Perhaps the problems seen in Fig. 3.3 can be partly explained by reference frame (RF) realization error, i.e. subtle differences between the realization of nominally identical RFs – the four RFs used to express the orbits of the altimeters, and the RF used to express the vertical motion of any tide gauges used in the altimeter calibration process. But we doubt that this could be the dominant contributor to the discrepancies seen in Fig. 3.3. There are several forms of calibration error, e.g. the water vapor radiometer calibration, or even the tide gauge input into the calibration process

being in some way incorrect or misrepresentative (e.g. an RSL time series was affected by an earthquake, but this was not recognized and corrected for).

We show this result, even though we do not seek to explain it in any detail, because it exemplifies the need to be as careful as possible when using tide gauges and nearby GPS stations to calibrate satellite altimeters.

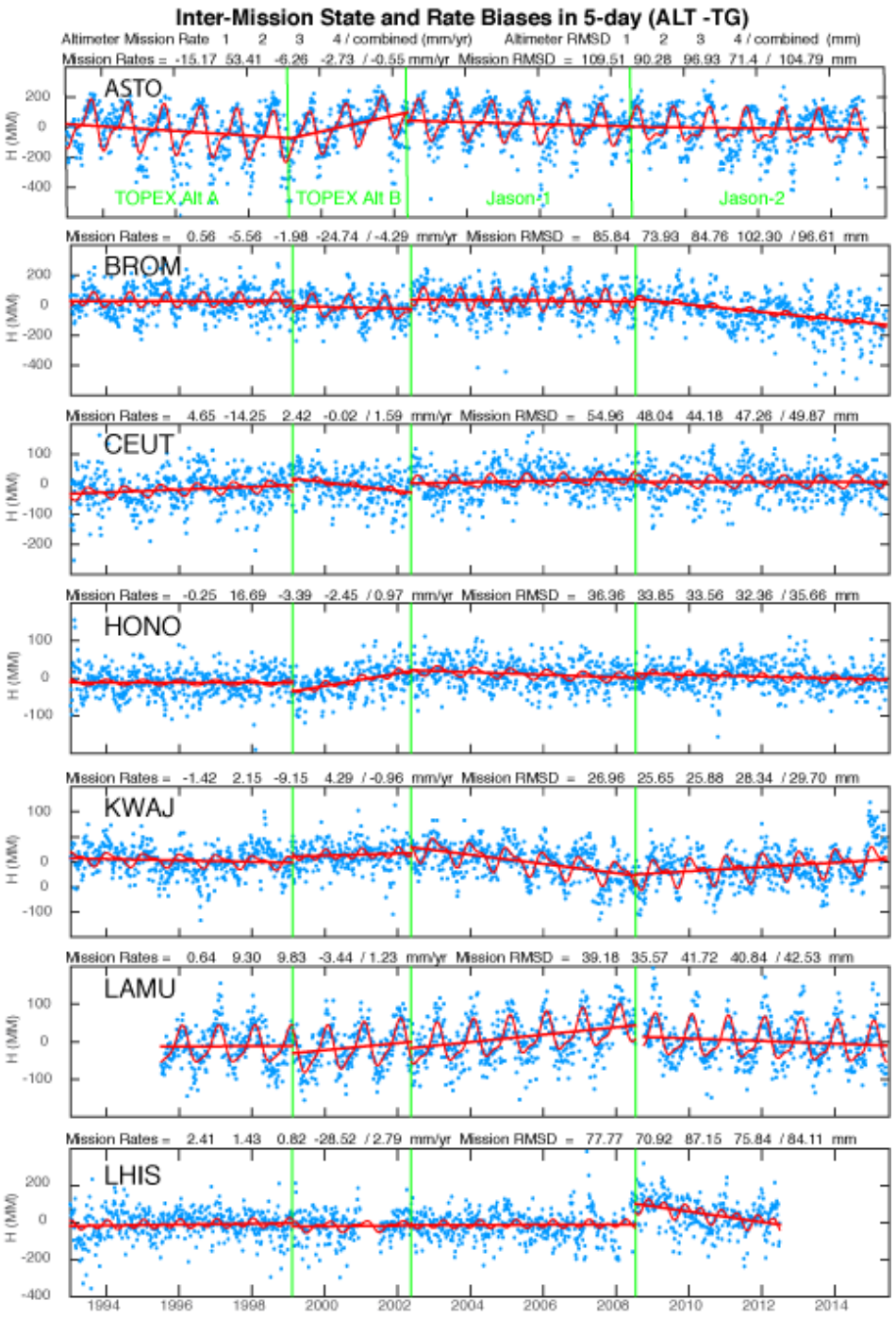

Figure 3.3 ALT-TG time series for 7 tide gauges. The change-over times between altimeter missions are shown with green lines. This uses the Beckley et al. (2016) solution for ASL.

Chapter 4. Estimating RSL rates at tide gauge PAGO

4.1 Estimating RSL rates at PAGO without mitigating the impacts of ocean dynamics

The most naïve estimate for the rate of RSL rise at PAGO would be that based on fitting a straight line, or an SLTM consisting of a linear trend plus an annual cycle, to the entire RSL time series (after ocean tides have been removed). This data set and an SLTM with a linear trend are depicted in Fig. 4.1 (a). The effect of the 2009 earthquake is quite apparent when looking at the entire time series (i.e. since ~ 1950), though it is rather less obvious if we restrict ourselves to a shorter time period (e.g. since ~ 1993) and have less confidence in the linear trend. The coseismic jump and postseismic transient of the 2009 earthquake perturbed RSL upwards, which means that the rate estimate of 3.12 1.8 mm/yr has a positive bias. We fit the same RSL time series with an ELTM in Fig. 4.1 (b), and this effectively 'insulates' the linear trend from the seismic perturbation by modeling that perturbation separately by evoking a jump and a logarithmic transient. This produces a substantial drop in the estimated rate, which is now 2.10 0.7, and reduced the RMS scatter from 75 mm to 67 mm. Note that the rates, coseismic jump amplitude (J) and the cumulative transient displacements (CTD), for these trajectory models, and subsequent trajectory models, are listed in Table 4.1.

Using a linear trend (i.e. constant rate) model to estimate the rate of RSL rise since ~ 1950 is obviously problematic given that there is an abundance of evidence that the RSL

rate is increasing with time (Chen et al., 2017; Nerem et al., 2018), along with the pace of global warming. There are two ways to address this rate variability: (i) produce linear fits in different time windows, and (ii) adopt a trend model which is polynomial in time, and thus estimate the change of rate in a time-continuous sense. If we are interested in the mean rate of RSL rise in the model altimetry era (1993.16 onwards) for example, we could fit the RSL data only in that time period. On the other hand, we could fit a polynomial trend model to the entire RSL time series, and then evaluate the mean rate in the time period of interest. The problem of using the shorter time period is that RSL time series are very noisy and the shorter the time period the less noise averaging occurs, and therefore the greater the random error in the rate estimates. In effect the conundrum is this: which is better - reduced random error but the possibility of a large systematic error if we use the much longer time series, versus increased random error (but greatly reduced systematic error) in the RSL rate estimates inferred from the much shorter time series? The systematic error or bias that we refer to is that which arises when we do not account for significant accelerations in RSL rate.

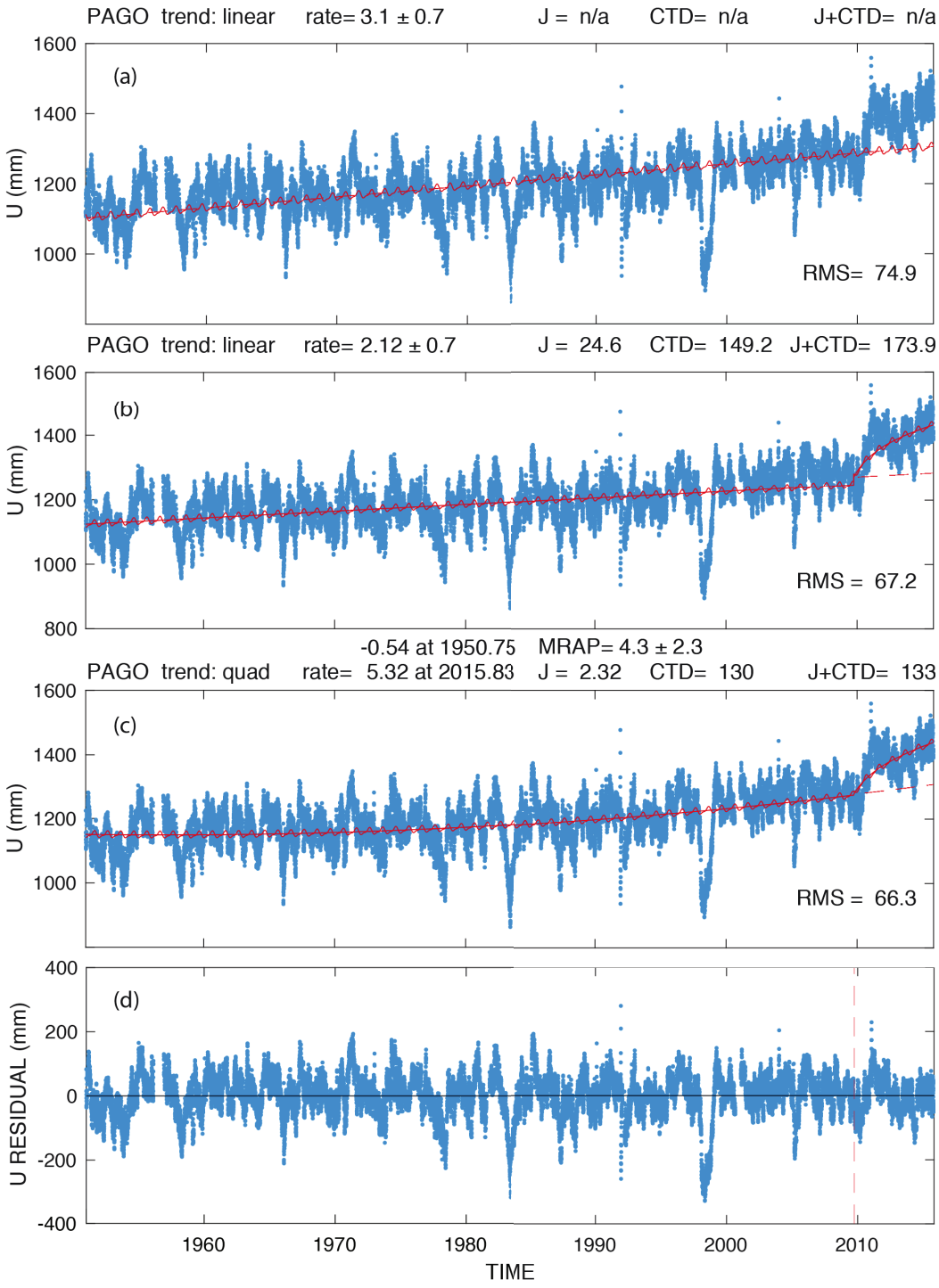

Figure 4.1 Trajectory models for RSL at PAGO from 1950.8 onwards (a) An SLTM with a linear trend that takes no account of the 2009 earthquake. (b) An ELTM that models the coseismic jump and postseismic transient, and assumes a linear trend. (c) An ELTM that invokes a quadratic trend. This is used to predict the mean rate in the altimeter period (MRAP). (d) The residuals from (c) – notice their asymmetry. The strong negative excursions are El Niño events.

We fit the PAGO time series with an ELTM featuring a quadratic or 'constant acceleration' trend model in Fig. 4.1 (c). The rate of a quadratic model changes linearly in time, from -0.54 mm/yr to 5.32 mm/yr. The mean rate in the time interval for our multi-altimeter solution (1993.16 – 2015.8) is 4.3 2.3 mm/yr. The residual time series (i.e. observed – model RSL) is shown in Fig. 4.1 (d), and it immediately raises another significant problem. The residuals have a highly asymmetric distribution around zero. The strong negative excursions, which are caused by El Niño events, are not balanced by similarly strong positive excursions. Such a skewed distribution of residuals has the potential to bias estimates of RSL rate (positively or negatively depending on the distribution of El Niño events in the time window of analysis). To avoid possible estimation bias we have to find some way to suppress the ocean dynamic noise. Note that dynamic variations in sea surface height (SSH) affect both ASL and RSL – and do so equally.

4.2 Estimating RSL rates at PAGO using an ocean climate index

In general terms, our approach to reducing biases in our RSL rate estimates is to attempt to 'insulate' the rate estimates from biases driven by dynamic SSH variations by modeling the SSH variability separately, just as we did with coseismic jumps and postseismic transients. This approach is often referred to as 'modeling out' a given noise source. We will attempt to do this with physical models of sea surface dynamics in the next section of this chapter. But first we attempt to achieve the same goal using the slightly cruder approach of predicting dynamic SSH variability using an ocean climate

index. The one significant advantage of using one or more oceanic indices to 'model out' dynamic ocean noise is that these indices are widely available from 1950 onwards.

In different parts of the world one would use different indices, or different combinations of indices, as a basis for predicting much of the dynamic variability of SSH. In the case of Samoa, the dominant signal is from ENSO, so we will focus on an ENSO index. The idea is to augment the design matrix associated with the ELTM by incorporating new basis functions derived from the index. We have experimented with two approaches: first we assumed that part of the oceanic dynamic signal in PAGO RSL time series can be predicted using a time-lagged time series of a standard ENSO index. Specifically, we assume the presence of RSL fluctuations that vary as some polynomial function of the optimally lagged index. The tide gauge specific task is to determine the order of the polynomial, and the optimal time lag. The second approach was to assume that RSL variability can be predicted using a Hilbert transform of a suitable ENSO index time series. We obtained a greater reduction in RMS misfit using the former approach, so we restrict our attention to the first approach in this thesis.

We begin by selecting a specific ENSO index and de-trending it. We represent the de-trended time series as $I(t)$. We assume that there exists some time lag τ such that $I(t+\tau)$ can be used to predict part of the ocean dynamical variability in RSL as a function of t. We tried to augment the ELTM for RSL at time t with basis functions $I(t+\tau)$, $I^2(t+\tau)$, and higher order powers of $I(t+\tau)$. We had better results using both $I(t+\tau)$ and its square rather than $I(t+\tau)$ alone, but we obtained no significant additional advantage when we

incorporated even higher powers. We searched over a wide range of time lags to determine the specific time lag that produced the best fits to the RSL time series. We did this using several different ENSO indices, and we obtained the best results using the index *OceanNino*. The time lag arises because different ENSO indices are tuned to specific sub-regions of the Pacific, and since the El Niño propagates from west to east, the drop in sea level driven by El Nino will occur earlier (later) than the drop in the ENSO index if the tide gauge lies west (east) of the index reference point. In the case of the tide gauge PAGO, which lies west of the 'center of mass' of the OceanNino region, the optimal lag is -0.453 years if we use a linear trend model and apply it to the entire time series (Fig 4.2). Since τ is an adjustable parameter, we have increased the number of degrees of freedom in the ELTM by 3, and this results in a 18.8 % drop in the RMS misfit of the data and model (Fig. 4.3a). The height residuals are far less skewed than previously (Fig. 4.3b). The estimated rate of RSL change is 2.12 0.51 mm/year, as opposed to 2.08 0.70 mm/yr when we made no use of the ENSO index OceanNino (Fig 1.8.3) to model the same RSL data set under the assumption of a linear trend. That is a very minor rate change, which is probably fortuitous. But using the index to augment the trajectory model reduced the RMS scatter by 19%, and it reduced the standard error on rate by 29 %.

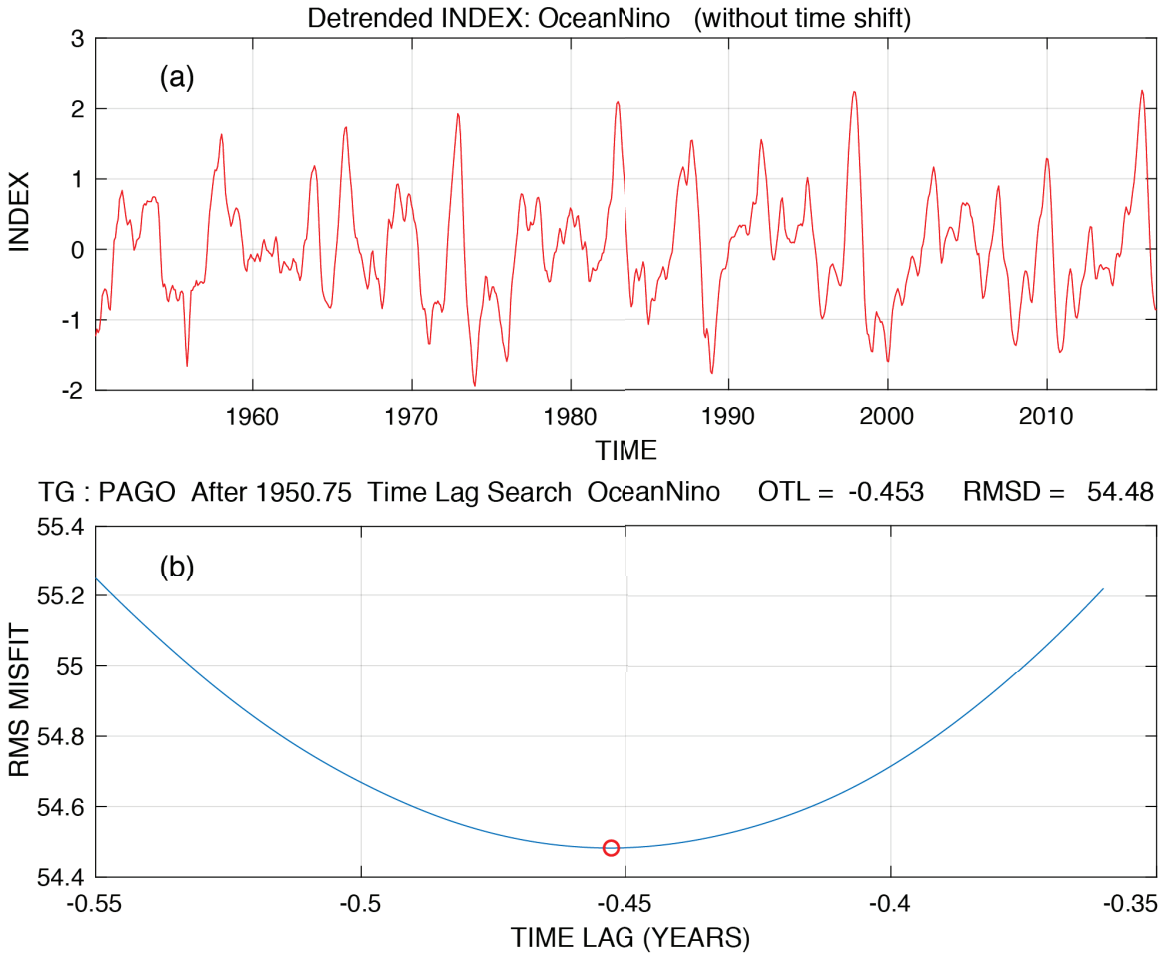

Figure 4.2 (a) The detrended ocean climate index OceanNino used (with an optimal time shift) to augment the design matrix of the ELTM. The time shifted index and its square are adopted as basis functions that can be used to predict dynamic SSH variations, and so insulate the ELTM parameters from their influence. (b) The search for an optimal time lag for the ELTM, with a linear rate, used to produce Fig. 4.3.

The search for an optimal time lag has to be repeated when any change is introduced in the ELTM, e.g. if we change the trend model from linear to quadratic. The fit obtained using a quadratic trend as well as the ocean index is shown in Figure 4.4, along with the comparison of the residual distributions when we invoke quadratic trend with and without the use of the ocean index. Again, the residuals obtained using the augmented trajectory model are less skewed.

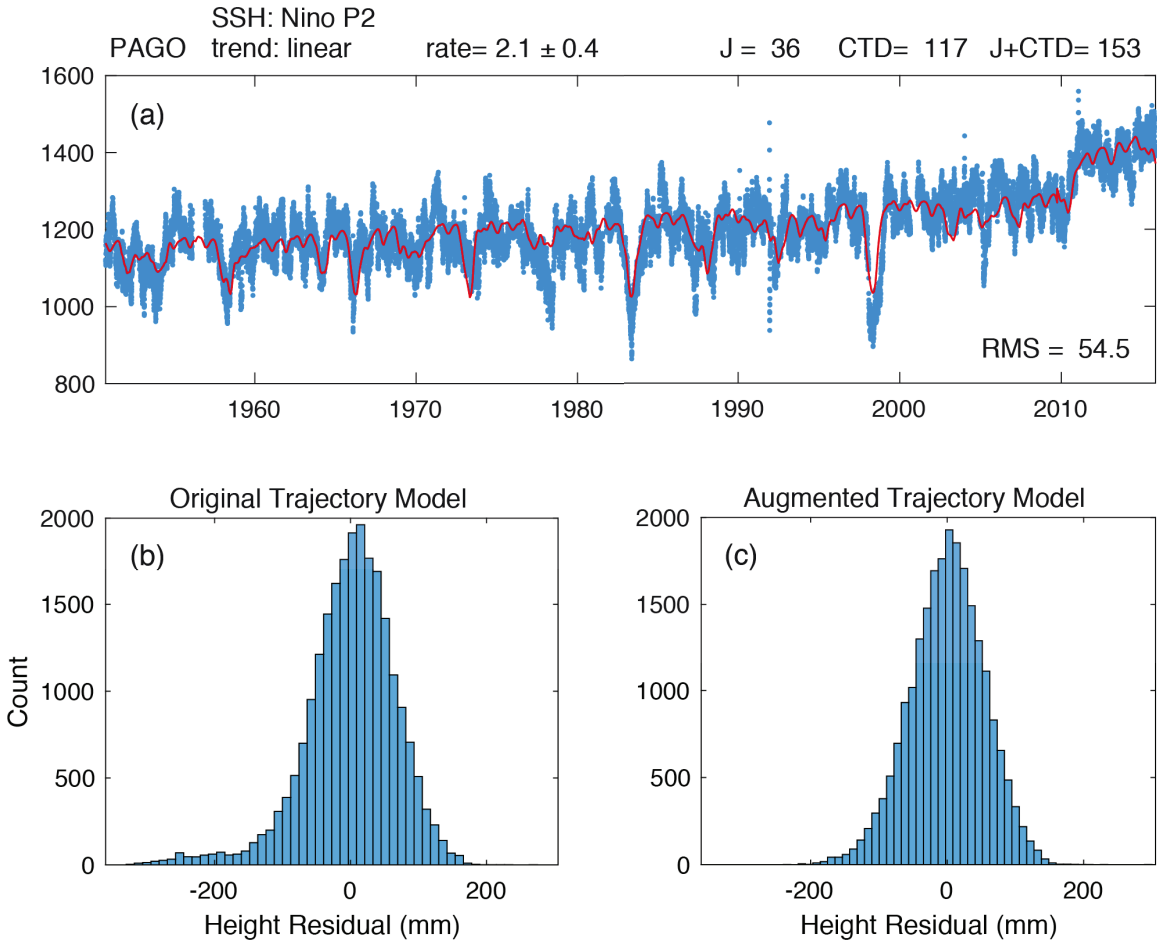

Figure 4.3 Trajectory models for RSL with Nino-linear at PAGO from 1950.8 onwards (a) The same time series that appeared in Fig. 4.1 (a-c), fit with an ELTM that invokes a linear trend but which has been augmented by two basis functions derived from an optimally-lagged OceanNino index. Note that the augmented model is now following the large negative excursions associated with El Niño events, reducing the size of the misfit. This suppresses the influence of the dynamic SSH variations on the rate parameter of the ELTM. (b) The residuals associated with the same ELTM, but without the augmentation (Fig 4.1b) – note their extreme asymmetry. (c) The residuals produced when the ELTM is augmented using the OceanNino index. The residuals are now much less skewed.

The rate now changes from 0.05 mm/yr at 1950.75 to 4.51 mm/yr at 2015.83, which differs substantially from the results obtained using a quadratic trend model without augmentation (Fig. 4.1c). The mean rate in the altimeter period (MRAP) when we use the climate index is 3.0 1.7 mm/yr whereas without augmentation we found an MRAP of 4.3 2.3 mm/yr.

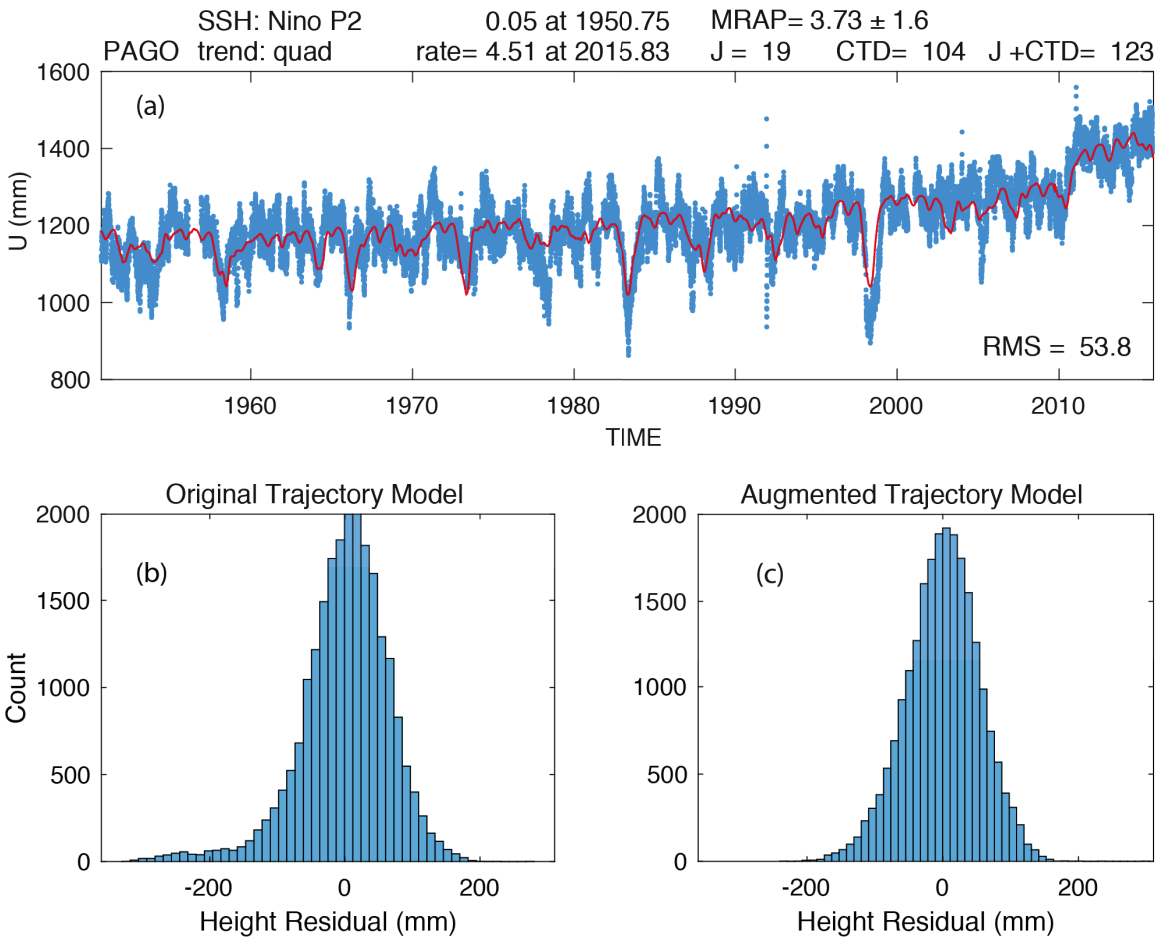

Figure 4.4 Trajectory models for RSL with Nino-quad at PAGO from 1950.8 onwards (a) PAGO RSL fit with an ELTM that invokes a quadratic trend and has been augmented by two basis functions derived from an optimally-lagged OceanNino index. This fit produces the residuals shown in (c), which contrast with the residuals (b) which occur without model augmentation (i.e. the residuals from the fit shown in Fig. 4.1(c)).

4.3 Estimating RSL rates at PAGO using a dynamic SSH model

The use of a physics-based ocean dynamics model driven by large numbers of observations is clearly preferable to using a simple ocean climate index. The only real disadvantage of using a numerical ocean dynamics model is that these models are more restricted in time. Most of them do not make predictions for the ocean state prior to about 1979. Still, that is well before TOPEX was launched and the modern altimetry era began.

We examined the ocean dynamics models CFSR (Saha et al., 2013), PEODAS (Hudson et al., 2012; Miles et al., 2014; McIntosh et al., 2015)) and ORA-S4 (Balmaseda and Mogensen, 2013). These models capture sea level variations associated with dynamic height changes, barotropic circulation, advection and dissipation processes. They deliver SSH histories on spatial grids. We used these models to predict SSH time series at our tide gauges and used these time series to augment our ELTM using an approach similar to that adopted with the ocean climate index. As before, we must remove any linear trend from the SSH predictions since we want the ELTM to absorb the linear trend *in toto*. We retained a search over possible time lags, and the optimal time lag was always small, as expected. We obtain the best results using ORA, and we show only those results in this thesis.

Dynamic SSH predictions made using ORA are available only for 1979 onwards, so all the results we show in this section are for that time period. In order to assess the impact of the ORA-augmented trajectory models we must compare it with an otherwise similar analysis for the same time period, and using the same ELTM.

Rather than showing the augmented model with the RSL dataset, in the remaining figures we remove the best-fit ORA sub-model from the data and display that data fit only with the ELTM sub-model. This provides us with a rather more vivid demonstration of the ORA model's ability to predict and remove dynamic SSH 'noise'. In each of the next three figures the raw RSL appears in the top subplot and the RSL minus the ORA SSH model appears in the bottom subplot.

We begin by invoking an ELTM with a linear trend (Fig. 4.5). Augmenting the ELTM with ORA (Fig. 4.5b) resulted in a 51% reduction in RMS scatter relative to the same ELTM without the use of ORA (Fig. 4.5a). Without ORA augmentation the rate is 3.81 1.63 mm/yr, but with ORA augmentation the rate drops to 3.37 0.56 mm/yr, which has a far smaller standard error.

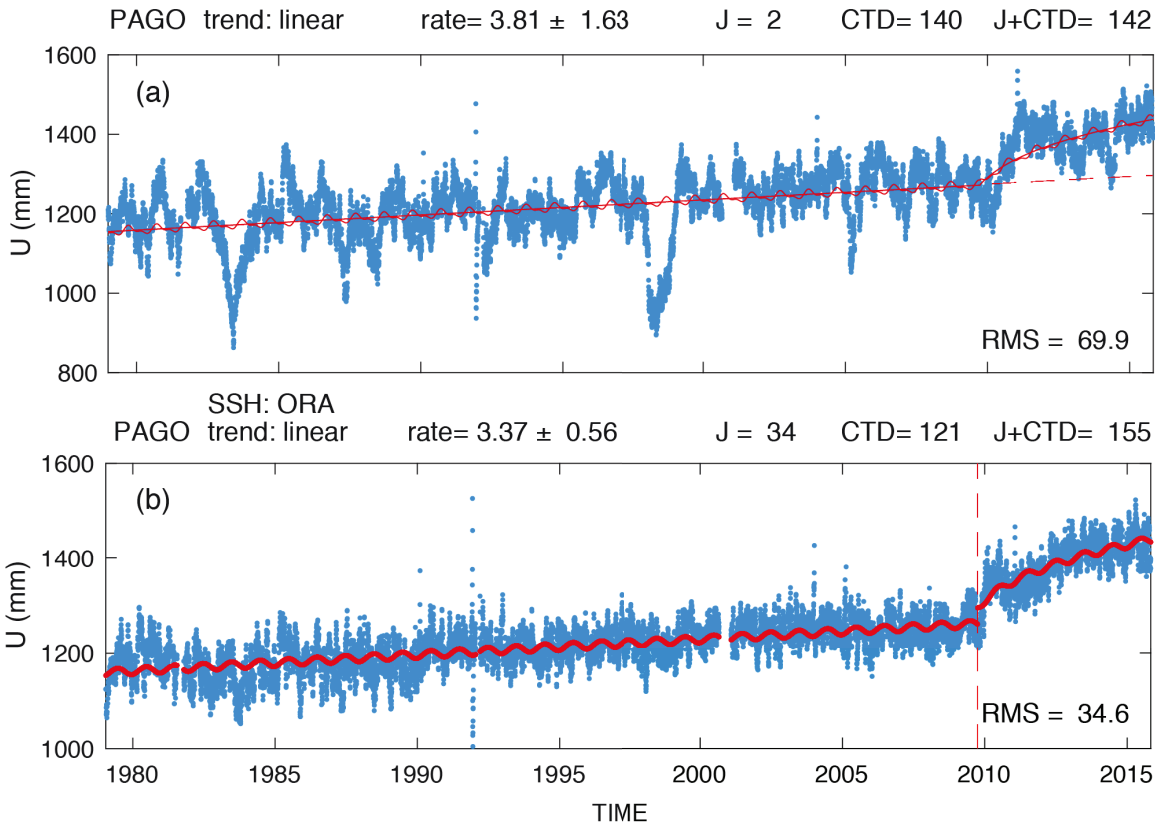

Figure 4.5 (a) The RSL time series at PAGO, after 1979, fit using an ELTM with a linear trend, without augmentation with the ORA model. (b) The RSL time series, after the optimal ORA model has been estimated, then removed from the RSL data, and the fit that is achieved using the remaining ELTM, which has a linear trend.

We repeat this process using a quadratic trend in Fig 4.6. Note that the reduction in RMS scatter (with ORA correction) for the quadratic case is very similar to that found previously for an ELTM with a linear trend. Both the initial rate and final rate values differ, as does the mean rate for the altimeter period (MRAP), i.e. 6.7 4.1 mm/yr without ORA versus 3.7 1.4 with ORA. Again, note the major reduction in the standard error for the MRAP estimate. Utilizing ORA dropped the RMS scatter level by 50%.

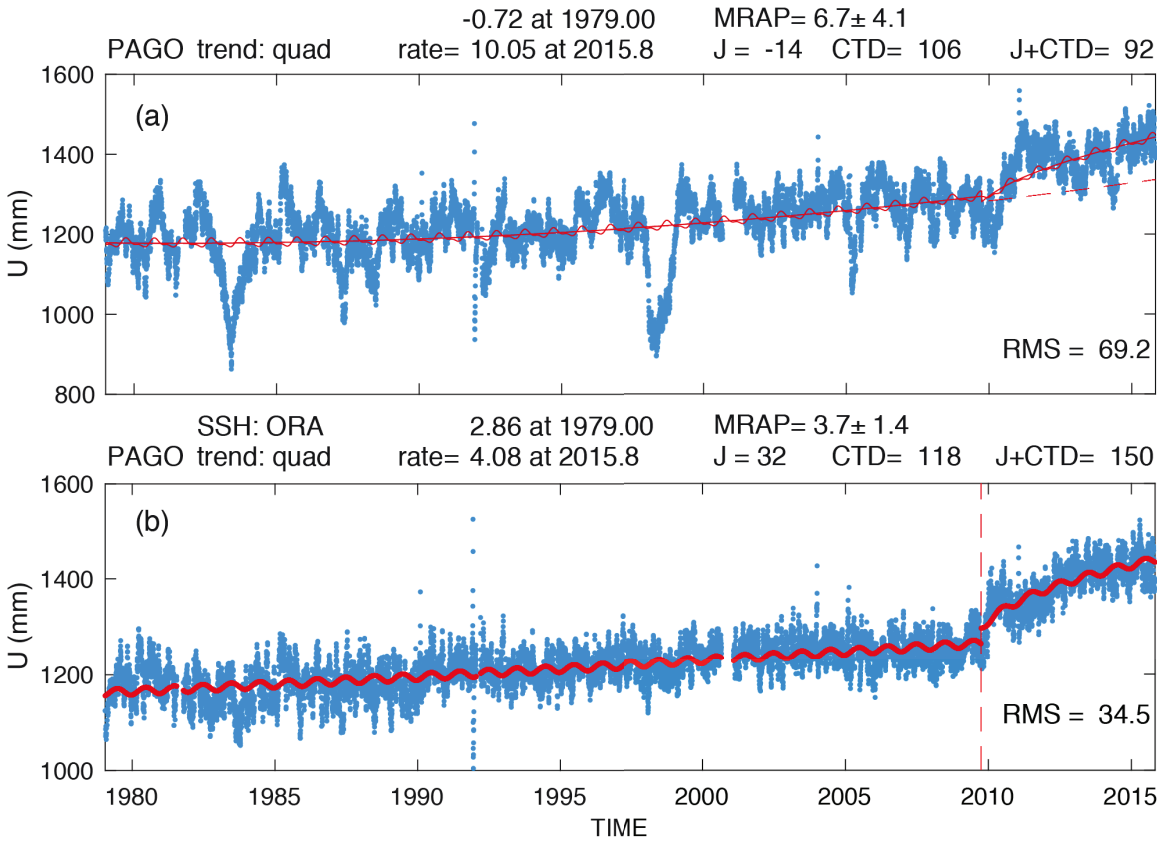

Figure 4.6 The RSL time series at PAGO, after 1979 fit with quad, (a) fit using an ELTM with a quadratic trend, without augmentation with the ORA model. (b) The RSL time series, after the optimal ORA model has been estimated, then removed from the RSL data, and the fit that is achieved using the remaining ELTM, which has a quadratic trend.

Finally, we perform the same analysis but after restricting the time window to 1993.16 onwards so as to estimate the RSL rate within the altimeter time period (Fig.4.7) based only on a linear trend. The rate without ORA is 6.3 3.2 mm/yr, whereas the rate with ORA augmentation is 3.94 0.94 mm/yr. The RMS scatter dropped by 56% and the standard error dropped by about 70%.

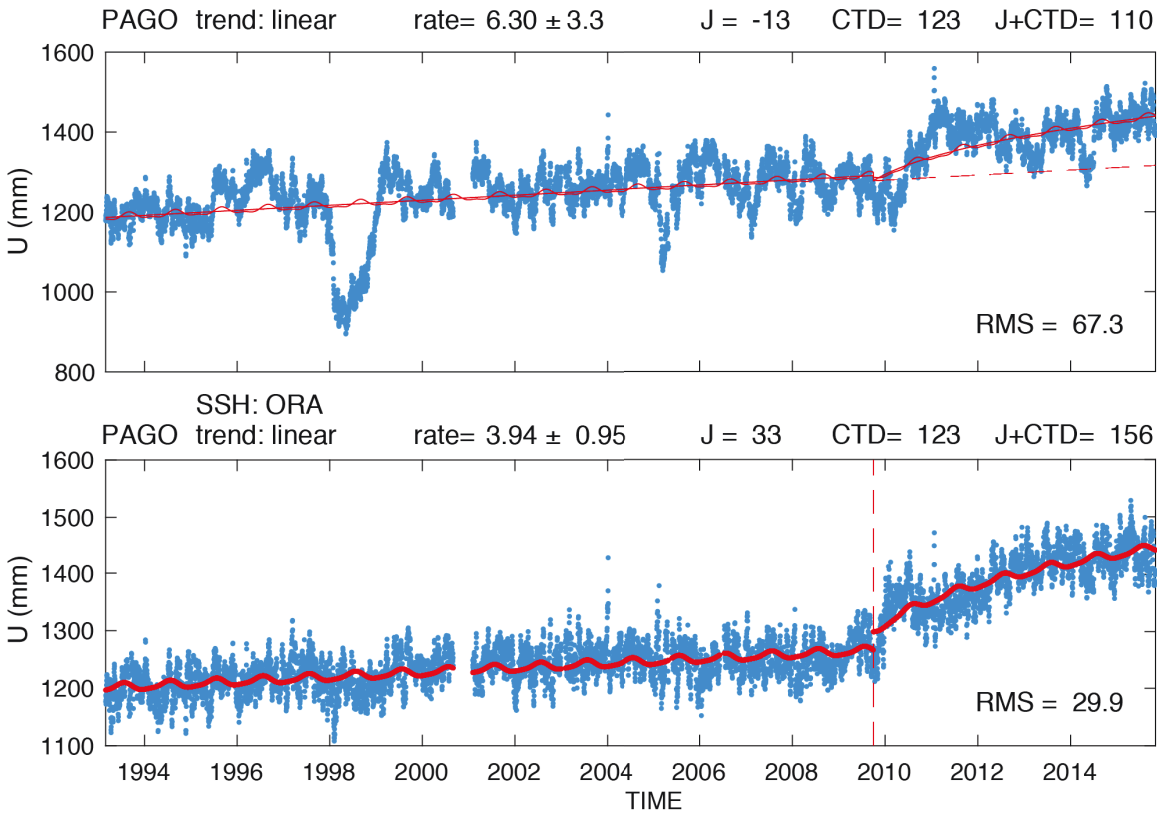

Figure 4.7 (a) The RSL time series at PAGO, during the altimetry period, fit using an ELTM with a linear trend, without augmentation with the ORA model. (b) The RSL time series, after the optimal ORA model has been estimated, then removed from the RSL data, and the fit that is achieved using the remaining ELTM, which has a linear trend.

All these results are summarized in Table 4.1

Table 4.1 Estimates of the RSL rate at Pago tide gauge based on a variety of modeling strategies, and associated estimates of other quantities of interest. The ORA model for dynamic SSH is not available before 1979. Those RSL rate estimates we consider plausible are bold-faced, but note that they may apply to different time periods.

Time span used for RSL	ELTM trend model	Dyn. SSH model	RSL rate (mm/yr) 'constant'	MRAP (mm/yr)	Jump (mm)	CTD (mm)	J+CTD (mm)	RMS sctr (mm)
1950.75 - 2015.8	linear	none	3.14 .70		n/a	n/a	n/a	75.0
1950.75 - 2015.8	linear	none	2.12 .70		24.6 53.1	149.2 71.2	173.9 49.1	67.2
1950.75 - 2015.8	quad	none		4.29 2.25	2.3 40.9	130.5 73.7	132.9 55.2	66.3
1950.75 - 2015.8	linear	Nino	**2.08 ± .53**		36.4 40.9	117.1 54.4	153.4 37.1	54.5
1950.75 - 2015.8	quad	Nino		**3.73 ± 1.66**	18.7 39.6	104.4 54.7	123.1 41.2	53.8
1979.0 - 2015.8	linear	none	3.81 1.63		1.7 56.1	140.3 78.6	142.1 57.0	69.9
1979.0 - 2015.8	linear	ORA	**3.37 ± .56**		34.3 20.6	121.3 29.0	155.6 20.0	34.6
1979.0 - 2015.8	quad	none		6.74 4.11	-13.9 54.9	106.1 90.0	92.1 77.2	69.3
1979.0 - 2015.8	quad	ORA		**3.72 ± 1.43**	32.5 20.5	117.5 32.9	150.2 27.6	34.5
1993.16-2015.8	linear	none	6.30 3.32		-13.1 53.7	123.1 82.7	110.0 65.7	67.4
1993.16-2015.8	linear	ORA	**3.94 ± .95**		32.2 16.2	122.5 24.3	155.7 18.7	29.9

For all ELTMs above, the timescale parameter for the logarithmic transient is 1.0 year.

MRAP rate, reported only when the trend model is quadratic, is the mean RSL rate predicted for the time interval 1993.16 -2015.8

Cum. transient refers to cumulative transient uplift in the interval between the earthquake and the end of the time series (2015.8).

J+T refers to the total displacement produced by the coseismic jump plus the logarithmic transient through 2015.8.

The last three columns above can be compared to the estimated parameters of an ELTM fit to the ASPA GPS time series (Fig 2.2a)

i.e. a jump of -25.6 mm, and cumulative transient displacement thru 2015.8 of -118.2 mm, and their sum -143.9 mm.

4.3 Estimating RSL rates by removing the seismic perturbations using a nearby GPS station

So far, we have tried to 'insulate' the RSL rate estimates from seismic perturbations by estimating the coseismic jump and the postseismic transient from the RSL time series themselves. In this section we take an alternative approach, and use the best fit jump and transient models obtained from nearby GPS stations to (nominally) remove the seismic perturbation from the RSL time series. This requires us to account for the change in sign between RSL and VLM perturbations. This allows us to estimate RSL rate using an SLTM instead of an ELTM (Chapter 1). We could do this with or without augmenting the SLTM design matrix using ORA, but given the successes obtained above, we choose to continue with ORA model augmentation. That is, the following three analyses (Fig. 4.8 and Table 4.2) remove the seismic perturbation using GPS, and model out dynamic SSH variability using ORA.

We begin by modeling the time series from 1979 onwards using a linear and quadratic trend model (Fig 4.8 a,b). The SLTM with a linear trend has a rate of 3.39 0.55 mm/yr. The SLTM with a quadratic trend has rate varying from 2.7 mm/yr at 1979 to 4.4 mm/yr at 2015.8, with the MRAP = 3.86 0.77.

We also compute the rate within the altimeter period based only on the data from that period of time (Fig. 4.8c). We find a rate of 4.05 0.86 mm/yr. We summarize these results in Table 4.2.

Table 4.2 Estimates of RSL rate at PAGO when the seismic perturbation is removed from the RSL time series using the geodetic estimates of the coseismic and postseismic transient uplift estimated at the nearly co-located GPS station ASPA. The quantities listed are defined as they were in Table 4.1.

Time span of RSL observations	SLTM trend model	Dynamic SSH model	RSL rate 'constant' (mm/yr)	MRSL rate in altimeter era (mm/yr)	RMS Scatter (mm)
1979-2015.8	linear	ORA	**3.54 ± 0.41**		34.62
1979-2015.8	quadratic	ORA		**3.86 ± 0.77**	34.54
1993.16-2015.8	linear	ORA	**4.30 ± 0.56**		29.96

The rates shown in rows 2-4 of this table can be compared to those in rows 5, 7 and 9 in Table 1.

Whereas the ELTM trajectory models used for Table 1 invoked a single timescale logarithmic transient model for RSL, the logarithmic transient model fitted to GPS U time series at ASPA was a double transient model that invoked transients with characteristic timescales of 0.0523 and 1.0 years.

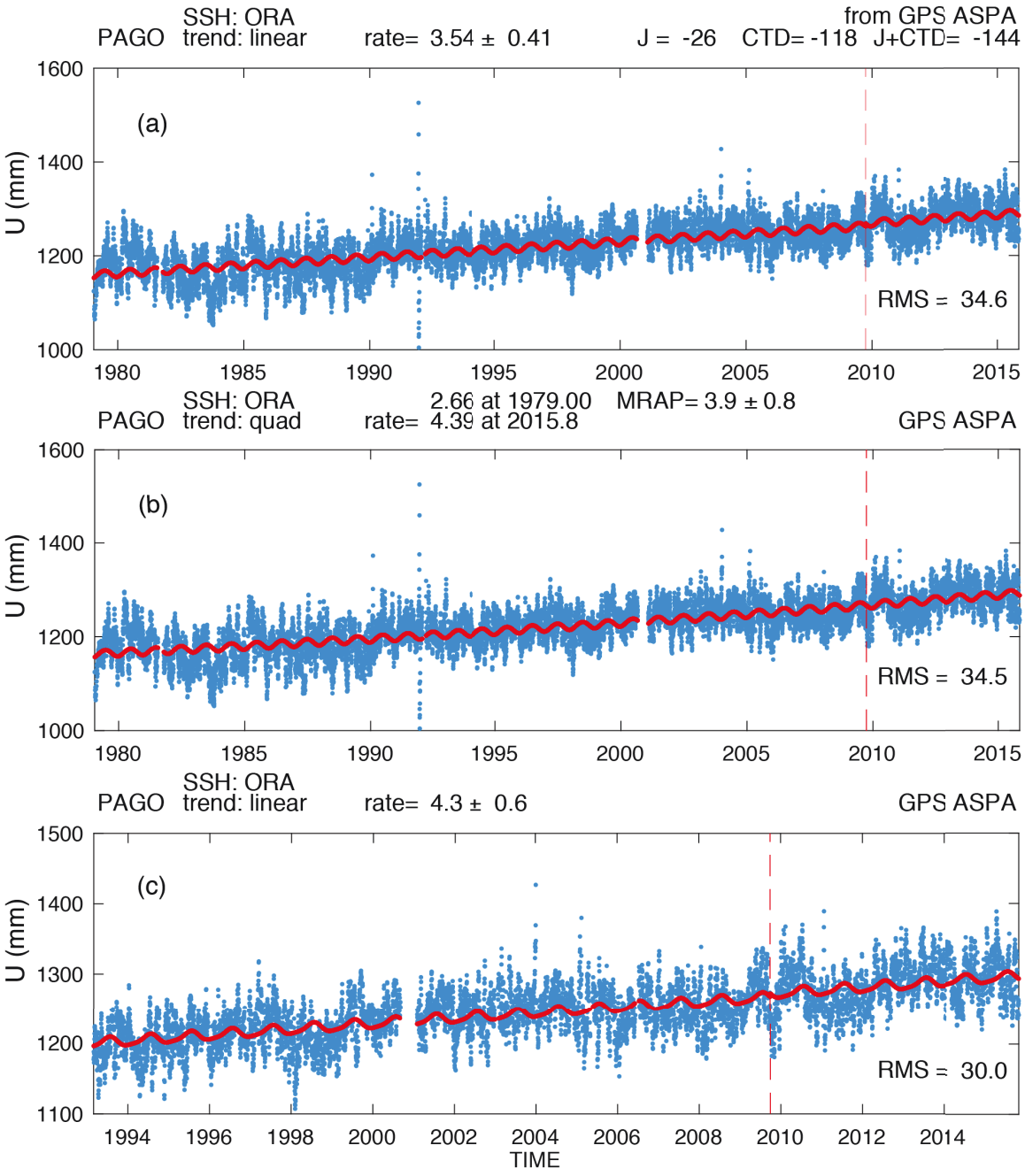

Figure 4.8 The RSL time series at PAGO in which the perturbation produced by the 2009 earthquake has been removed by applying the coseismic jump and postseismic transient solution obtained at nearby GPS station ASPA. All three models shown are SLTMs augmented by ORA. Here we remove the optimal estimates of dynamic SSH variations from the model and the data, so that only the SLTM component of the model remains. (a) An SLTM with a linear trend, from 1979 onwards. (b) An SLTM with a quadratic trend, from 1979 onwards. (c) a SLTM with a linear trend, from 1993 onwards.

4.4 A meta-analysis of mean RSL rates over different time spans

When we examine the results summarized in Tables 4.1 and 4.2, we must keep in mind that whenever the ELTM or SLTM invoked a linear trend, the RSL rate estimate refers to the mean rate over the time span of the RSL data. If the sea level rise is accelerating at a constant rate, then the mean rate associated with each time window should increase in proportion to the time at the center of the time window. When we invoke ELTMs and SLTMs with quadratic trends, and estimate the mean rates in the altimeter period (MRAP), those estimates should be 'posted' at the mid-point of the altimeter time period (1993.16-2015.8). We plot all plausible estimates already derived in Fig. 4.9. We fit a line by weighted least squares (weighting each rate estimate using its standard error, as listed in Tables 4.1 and 4.2) and estimate an RSL acceleration rate of 0.094 0.040 mm/yr^2. This means that every decade the rate of RSL rise increases by about 0.94 mm/yr.

We have two other potentially useful estimates of RSL acceleration. These come from the quadratic ELTM models from 1951 onwards, one with no dynamic SSH correction, and the other corrected (or augmented) using a dynamic SSH model based on the climate index OceanNino. These acceleration estimates are 0.091 0.090 mm/yr^2 and 0.069 0.066 mm/yr^2, respectively. If we calculate a weighted average of these *direct* estimates of RSL acceleration since 1951, we arrive at an acceleration rate of 0.074 0.053 mm/yr^2. None of these three estimates is statistically incompatible with the rate of 0.094 0.040 mm/yr^2 from our meta-analysis of how mean rates have changed over time.

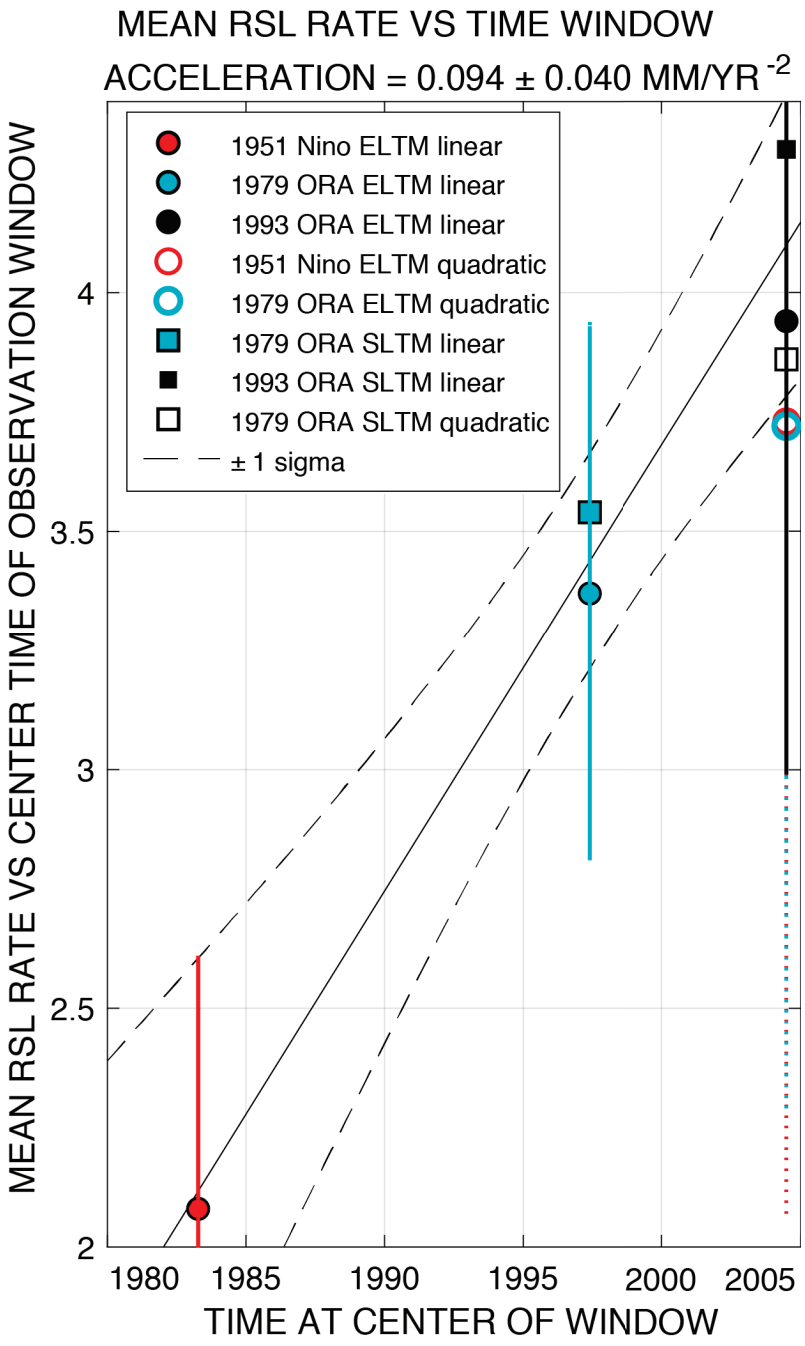

Figure 4.9 Estimating the acceleration rate of RSL at PAGO by estimating a linear relationship between the various estimates for mean RSL rate and the time at the center of the time window for each of these analyses. We have not plotted the error bars on the individual estimates, but they are always very large (Tables 4.1 and 4.2) compared even to the largest misfit in this plot. None of the points is significantly removed from the best fit line.

What first seemed a bewildering array of disparate estimates for RSL rate is actually remarkably consistent with an approximately constant acceleration, even though the assumption of constant acceleration was only built into three of the eight trajectory models used to estimate the rates shown in Fig. 4.9. Even the two rate estimates that do not fit as well as the others have 1-sigma error bars that overlap the best fitting line.

Of course, this plot is based on a meta-analysis, and the individual rate estimates are far from independent. Therefore the 95% confidence interval shown with the dotted lines is likely to be optimistic. If we calculate a weighted average of the three estimates nearest the top right corner of the plot, we would conclude that the MRAP = 4.10 0.41 mm/yr, and if we used all five estimates near the top right corner of the plot then we would conclude that MRAP = 4.06 0.38. (The best fitting line from our meta-analysis suggests MRAP= 4.01 0.32 mm/yr).

To err on the side of caution, we adopt the following estimate: MRAP = 4.06 ± 0.38 mm/yr.

We note in closing this section that the non-independence of the various rates in our meta-analysis means that the estimated acceleration rate of 0.094 0.040 mm/yr^2 surely has a very optimistic standard error estimate. However, we do notice that Nerem et al. (2018) recently estimated the rate of acceleration in global mean sea level (GMSL) rise for the time period from 1993-2016 as 0.084 0.025 mm/yr. There is no reason why regional acceleration rates in ASL should match the global rate, but it is rather gratifying

that this rate does not differ significantly (at the 95% confidence level) from either our 'direct' (0.074 0.053 mm/yr^2) or 'indirect' (0.094 0.040 mm/yr^2) estimates of RSL acceleration rates.

4.5 Estimating the mean rate of ASL rise in the altimeter period (1993.16-2015.8)

We can use Eq. 1.2 to estimate the mean ASL rate in the altimeter period by assuming that the rate of vertical motion at ASPA, -0.48 0.60 mm/yr, is a reasonable estimate of vertical crustal motion at PAGO. Since $V_{ASL} = V_{RSL} + V_{LM}$, if we set $V_{RSL} = 4.06$ 0.38 mm/yr and $V_{LM} = -0.48$ 0.60 mm/yr, then we conclude that

V_{ASL} = 3.58 ± 0.71 mm/yr at PAGO.

Our estimate for the mean ASL rate at PAGO is similar to the GMSL rate estimated by Nerem et al. (2018), which was 3.0 0.4 mm/yr. Again, there is no reason a regional mean ASL rate should match the global mean rate, but we note that the two estimates are not significantly different at the 95 % confidence level.

4.6 Discussion

We have illustrated a variety of problems that arise when we seek to estimate the rate of ASL rise at the tide gauge PAGO using the rate of RSL inferred from the tide gauge data, geodetic observations of VLM made by the nearby GPS station ASPA, and Eq. 1.1. We have shown that we can largely 'insulate' an RSL rate estimate from an earthquake-induced jump and transient signal in RSL by modeling those perturbations using an ELTM. One could achieve a similar result simply by eliminating all RSL data obtained on and after the day of this earthquake, but it is advantageous not to do so because we can compare the amplitudes of the coseismic jumps estimated from the tide gauge data and

using a nearly collocated GPS displacement time series, which enables a useful consistency check. Another advantage is the longer the time series the better able we are to calibrate a stochastic noise model which is essential for 'correcting' or renormalizing the standard error estimates.

Perhaps the greatest source of difficulty in using Eqs. 1.1 or 1.2 to estimate the rate of ASL rise at most tide gauges is that there are many plausible approaches to estimating the rate of RSL rise, and these methodologies produce significantly different results (Table 4.1 and 4.2). It seems to us that this problem will often be the major source of difficulty associated with the CGPS@TG agenda, even in some areas like PAGO, that have been affected by a single significant earthquake. The disparate RSL rate estimates can be resolved when we account for the presence of an acceleration in ASL rate and/or RSL rate. Any increase in ASL rate will propagate into RSL rate, but RSL rate might be affected by accelerating rates in VLM. This could be a major issue in places like Greenland, where accelerating crustal uplift is ubiquitous (Bevis and Brown, 2014).

Chapter 5. The Tale of Two Samoas

5.1 Estimating RSL rates at UPOL

We now focus our attention on the tide gauge UPOL in Apia, Samoa. This tide gauge is located close to the GPS station SAMO and on the same island as GPS station FALE. We have confidence in the stability of station SAMO because its long-term vertical velocity is very similar to that recorded by FALE, which is coupled to bedrock (Chapter 2). The only concern about the situation in Apia is that we know that UPOL sits on a harbor wall built on engineering fill, and this wall, and therefore UPOL, is subsiding (Chapter 3). We will have to correct for this engineering instability. Local near-surface subsidence means that RSL rise recorded by the gauge is greater than the RSL rise relative to the crust and lithosphere. That is, the RSL rate recorded by the gauge is larger than RSL for Apia as a whole.

The UPOL tide gauge was built and became operational in early 1993. Its time series is far shorter than PAGO's time series. It is far too short to support a meaningful estimate of RSL acceleration rates. But this is hardly necessary since UPOL's time series began almost at the opening of the altimetry era.

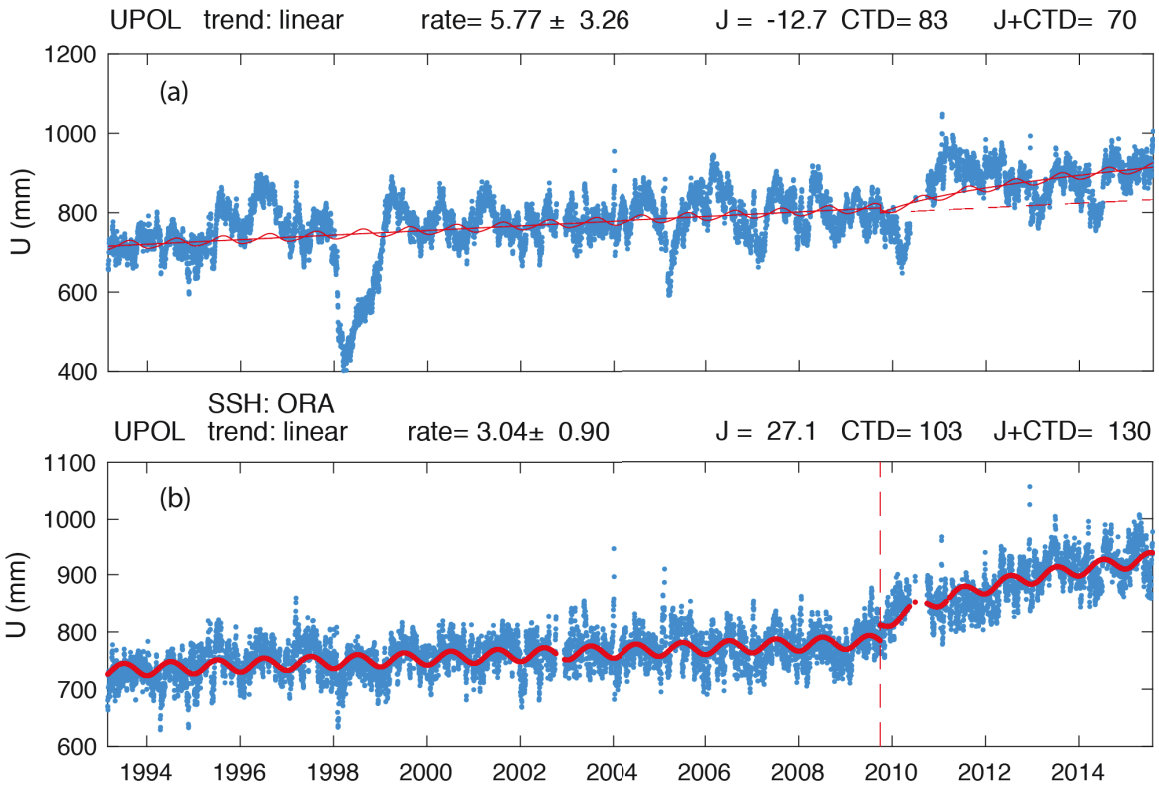

Figure 5.1 Fitting the raw (a) and (b) ORA-corrected RSL time series at UPOL with an ELTM featuring a linear trend. See Table 5.1.

We begin by fitting UPOL's RSL time series with an ELTM featuring a linear trend, without augmenting the trajectory model using ORA, as seen in Fig. 5.1 (a). Even though the rate estimate is at least partly insulated from the perturbation in VLM due to the 2009 earthquake, it is not insulated from the strong downwards excursion in sea level caused by the 1997/1998 El Niño event. As a result, this event 'pulls down' the left hand side of the trend line, biasing the rate estimate (5.8 3.3 mm/yr) in a positive sense. There is no point in trying to mitigate such dynamic SSH noise using the ocean climate index OceanNino. Because this time series is so short we can use the ORA model instead, and that is clearly the far better approach. We follow the same approach as we did in PAGO, fitting a composite SLTM and ORA model based by searching on an optimal time lag,

but then we remove the ORA component of the model from the original data, and show what remains and its fit with the SLTM (Fig. 5.1 b). Note that the 1997/98 El Niño excursion has been almost entirely 'modeled out' by ORA. The RSL rate estimate now drops to 3.04 0.90 mm/yr. But we note that this solution is underestimating the combined impact of the coseismic jump (J) and the cumulative transient displacement (CDT) at epoch 2015.8, which we designate J+CTD (Fig 5.1b and Table 5.1). We know this by comparing J+CDT estimated from this fit with J+CTD estimated at GPS station SAMO. The two sets of estimates ought to match apart from a change in sign. The fact that the fit seen in Fig. 5.1 (b) overestimates J+CTD by 44 mm/yr suggests that it may be underestimating the rate by 'pushing down' the right hand side of the linear trend.

Table 5.1 Estimates of the RSL rate at Upolo (UPOL) tide gauge based on a variety of modeling strategies, and associated estimates of other quantities of interest.

Time span used for RSL	ELTM trend model	Dynam SSH model	RSL rate (mm/yr) 'constant'	Jump (mm)	CTD (mm) 2015.8	J+T (mm) 2015.8	RMS sctr (mm)
1993.16-2015.8	linear	none	5.77 3.25	-12.7 53.4	82.8 83.0	70.1 65.7	68.47
1993.16-2015.8	linear	ORA	3.04 0.90	27.1 15.8	103.4 24.2	130.4 18.3	28.99

The last three columns above can be compared to the estimated parameters of an ELTM fit to the SAMO GPS time series (Fig 2.2b) i.e. a jump of -15.9 mm, and cumulative transient displacement thru 2015.8 of –70.2 mm, and their sum -86.1 mm.

Accordingly, we now take the alternative approach, as we did for PAGO, and remove the coseismic jump and transient from the UPOL RSL time series by using the jump and transients estimated by the nearly collocated GPS station SAMO. We can then fit the remaining time series with an SLTM with a linear trend augmented with a dynamic SSH model based on ORA. Having found the optimal time lag parameter we remove the ORA

sub-model from the data and show the fit of the ORA-corrected RSL time series and the SLTM (Fig. 5.2a). Note that the RSL rate has now increased to 4.40 0.59 mm/yr. Out of curiosity we do the same using the more remote GPS station FALE to correct for the coseismic jump and transient at UPOL, though it is clearly preferable to do this with SAMO, since it is located much closer to UPOL. The rate estimate increases to 5.27 0.63 mm/yr, because a FALE-based correction is underestimating the amplitudes of the coseismic jump and postseismic transient at UPOL. It is clearly better to use SAMO.

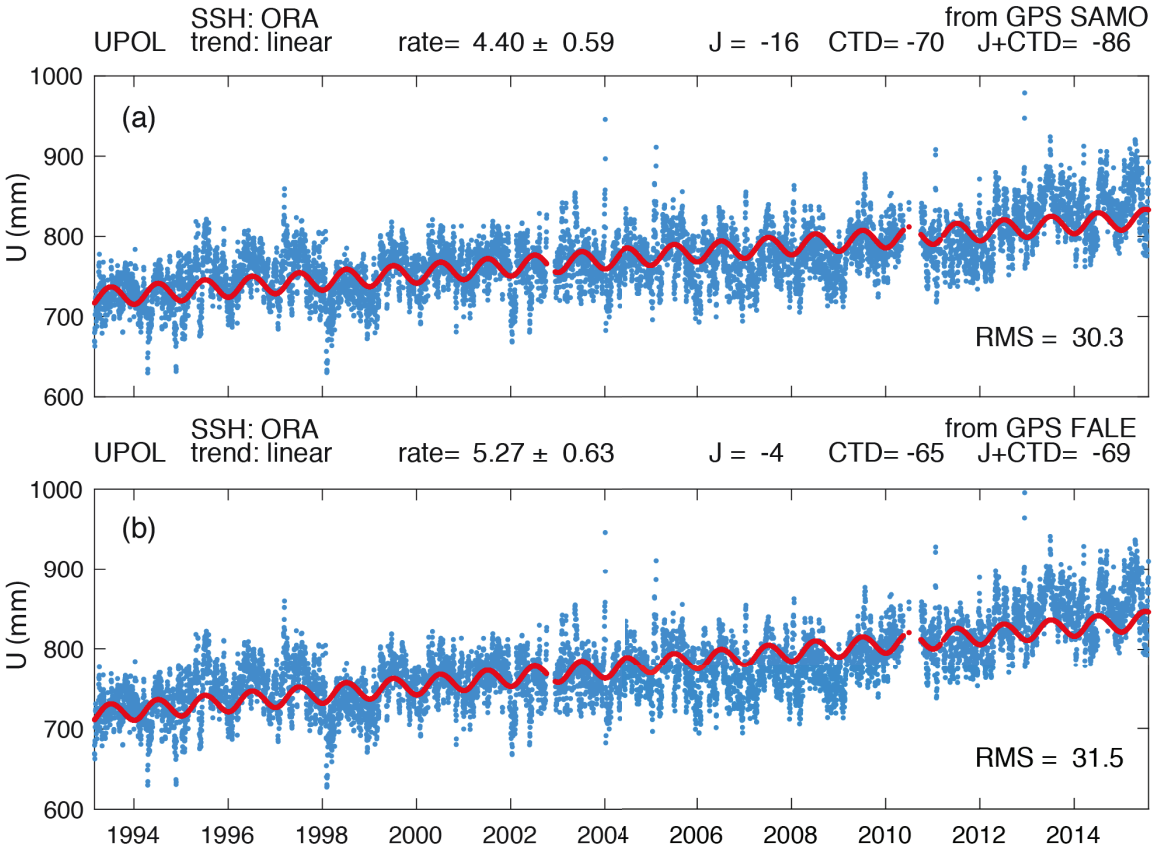

Figure 5.2 The fit of ORA-corrected RSL time series at UPOL with a SLTM featuring a linear trend, when the coseismic jump and posteismic transient are corrected using measurements from (a) GPS station SAMO, and (b) GPS station FALE. Solution (a) is preferred since FALE will underestimate the coseismic jump and transient at UPOL, and therefore overestimate RSL rate. See Table 5.2.

Table 5.2 Estimates of RSL rate at UPOL when the seismic perturbation is removed from the RSL time series using the geodetic estimates of the coseismic and postseismic transient uplift estimated at the nearly co-located GPS stations SAMO and FALE. The quantities listed are defined as they were in Table 5.1.

Time span of RSL observations	SLTM trend model	Dynamic SSH model	RSL rate 'constant' (mm/yr)	RMS Scatter (mm)	GPS
1993.16-2015.8	linear	ORA	4.40 0.60	30.0	SAMO
1993.16-2015.8	linear	ORA	5.27 0.63	31.5	FALE

The rates shown in this table can be compared to those in row 2 in Table 5.1.

Whereas the ELTM trajectory models used for Table 5.1 invoked a single timescale logarithmic transient model for RSL, the logarithmic transient model fitted to GPS U time series at SAMO was a double transient model that invoked transients with characteristic timescales of 0.0523 and 1.0 years.

Our preferred value for the rate of change of RSL at UPOL is 4.40 0.60 mm/yr. But this refers to the RSL rate at the gauge itself, which is subject to local subsidence. We know that the subsidence rate is -0.82 0.15 mm/yr. This implies that

the RSL rate at UPOL (~MRAP), referred to the lithosphere, is 3.58 ± 0.62 mm/yr.

5.2 Estimating the ASL rate at UPOL and for the two Samoas

We must now correct for the vertical motion of the lithosphere, using the vertical velocity of GPS station SAMO, -1.69 0.45 mm/yr, to arrive at an estimate for the rate of change of ASL. We find that

V_{ASL} = 1.89 ± 0.77 mm/yr at UPOL

We chose to use SAMO to correct for the vertical crustal velocity at UPOL because SAMO is much closer to UPOL than is FALE, and the tectonic signal is expected to be slightly different. But if we had used the vertical velocity of FALE, -1.86 0.26 mm/yr, then this would reduce the ASL rate at UPOL to 1.72 0.67 mm/yr.

Our estimate of 1.89 0.77 mm/yr for the ASL rate at UPOL should be compared with our previous estimate of the ASL rate at PAGO (3.58 0.71 mm/yr) which is 126 km from UPOL. The difference between the two ASL rates is 1.69 1.04 mm/yr, which is not statistically significant at the 95% confidence level.

The average of the ASL rate (V_{ASL}) estimates at UPOL and PAGO is 2.8 ± 0.5 mm/yr

similar to the post-1993 mean GMSL rates estimated by Hay et al. (2015), i.e. 3.0 0.7 mm/yr, and by Watson (2015) who estimated the mean GMSL rate using two different sets of VLM estimates and found rates of 2.6 0.4 mm/yr and 2.9 0.4 mm/yr. The weighted average of these three estimates of mean GMSL rate is 2.8 0.3 mm/yr.

Bibliography

Ablain, M., Cazenave, A., Valladeau, G., & Guinehut, S. (2009). A new assessment of the error budget of global mean sea level rate estimated by satellite altimetry over 1993-2008. *Ocean Science*, 5(2), 193-201.

Agnew, D. C., (1992). The time-domain behavior of power-law noises. *Geophysical Research Letters*, 19(4), 333-336.

Altamimi, Z., Sillard, P., & Boucher, C. (2002). ITRF2000: A new release of the International Terrestrial Reference Frame for earth science applications. *Journal of Geophysical Research: Solid Earth (1978–2012)*, 107(B10), ETG-2.

Altamimi, Z., Collilieux, X., Legrand, J., Garayt, B., & Boucher, C. (2007). ITRF2005: A new release of the International Terrestrial Reference Frame based on time series of station positions and Earth Orientation Parameters. *Journal of Geophysical Research: Solid Earth (1978–2012)*, 112(B9).

Altamimi Z, Collilieux X, Métivier L (2011) ITRF2008: an improved solution of the International Terrestrial Reference Frame. *Journal of Geodesy,* 85(8), 457–473.

Amiri-Simkooei, A. R., C. C. J. M. Tiberius, and P. J. G. Teunissen (2007), Assessment of noise in GPS coordinate time series: Methodology and results, J. Geophys. Res., 112, B07413.

Anzenhofer, M., Shum, C. K., & Rentsh, M. (1999). Coastal altimetry and applications. Ohio State University Geodetic Science and Surveying Tech. Rep,464, 36.

Arhan, M., & De Verdiére, A. C. (1985). Dynamics of eddy motions in the eastern North Atlantic. *Journal of physical oceanography*, 15(2), 153-170.

Balmaseda, M. A., Mogensen, K. and Weaver, A. T. (2013), Evaluation of the ECMWF ocean reanalysis system ORAS4. Q.J.R. Meteorol. Soc., 139: 1132-1161. doi:10.1002/qj.2063

Barbosa, S. M., & Andersen, O. B. (2009). Trend patterns in global sea surface temperature. *International Journal of Climatology*, 29(14), 2049-2055.

Beavan, J., X. Wang, C. Holden, K. Wilson, W. Power, G. Prasetya, M. Bevis, and R. Kautoke (2010), Near-simultaneous great earthquakes at Tongan megathrust and outer rise in September 2009, *Nature*, **466**, 959–963.

Beckley, B. D., Zelensky, N. P., Holmes, S. A., Lemoine, F. G., Ray, R. D., Mitchum, G. T., ... & Brown, S. T. (2010). Assessment of the Jason-2 extension to the TOPEX/Poseidon, Jason-1 sea-surface height time series for global mean sea level monitoring. *Marine Geodesy*, 33(S1), 447-471.

Beckley, B.; Zelensky, N.P.; Holmes, S.A.;Lemoine, F.G.; Ray, R.D.; Mitchum, G.T.; Desai, S.; Brown, S.T. (2016). Global Mean Sea Level Trend from Integrated Multi-Mission Ocean Altimeters TOPEX/Poseidon Jason-1 and OSTM/Jason-2 Version 4.2. Ver. 4.2. PO.DAAC, CA, USA.

Bergé-Nguyen, M., Cazenave, A., Lombard, A., Llovel, W., Viarre, J., & Cretaux, J. F. (2008). Reconstruction of past decades sea level using thermosteric sea level, tide gauge, satellite altimetry and ocean reanalysis data. *Global and Planetary Change*, 62(1), 1-13.

Bevis, Michael & Taylor, F & Schutz, B.E. & Récy, Jacques & Isacks, Bryan & Helu, Saimone & Singh, Rajendra & Kendrick, Eric & Stowell, James & Taylor, Brian & Calmant, Stéphane. (1995). Geodetic observations of very rapid convergence and back-arc extension at the Tonga arc. Nature. (374) 10.1038/374249a0.

Bevis, M., Scherer, W., & Merrifield, M. (2002). Technical issues and recommendations related to the installation of continuous GPS stations at tide gauges. *Marine Geodesy*, 25(1-2), 87-99.

Bevis M., Brown, A., and Kendrick, E. (2013). Devising stable geometrical reference frames for use in geodetic studies of vertical crustal motion, *Journal of Geodesy*, 87(4), 311-321.

Bevis, M. & Brown, A. (2014). Trajectory models and reference frames for crustal motion geodesy. *Journal of Geodesy*, 88(3), 283-311.

Bindoff N, Willebrand J (Coordinating Lead Authors) Artable V, Cazenave A, Gregory J, GulevS, Hanawa K, Le Quere C, Levitus S, Nojiri Y, Shum CK, Talley L, Unnikrishnan A (Lead Authors) and 50 contributing authors (2007) Chapter 5: observations: oceanic climate change and sea-level, *Intergovernmental Panel Climate Committee (IPCC) Working Group 1 (WG1) Fourth Assessment Report*

Bjornsson, H., & Venegas, S. A. (1997). A manual for EOF and SVD analyses of climatic data. *CCGCR Report*, 97(1).

Boening, C., Willis, J. K., Landerer, F. W., Nerem, R. S., & Fasullo, J. (2012). The 2011 La Niña: So strong, the oceans fell. *Geophysical Research Letters*,39(19).

Bonnefond, P., Exertier, P., Laurain, O., Ménard, Y., Orsoni, A., Jan, G., & Jeansou, E. (2003). Absolute calibration of Jason-1 and TOPEX/Poseidon altimeters in corsica special issue: Jason-1 calibration/validation. Marine Geodesy, 26(3-4), 261-284.

Bos, M.S., Fernandes, R.M.S., Williams, S.D.P., Bastos, L. (2008) Fast error analysis of continuous GPS observations, *Journal of Geodesy.* 82, 157–166.

Bos, M.S., Fernandes, R.M.S., Williams, S.D.P. et al., (2013). Fast error analysis of continuous GNSS observations with missing data. *Journal of Geodesy*. 87(4) 351–360.

Bosch, W., Dettmering, D., & Schwatke, C. (2014). Multi-mission cross-calibration of satellite altimeters: Constructing a long-term data record for global and regional sea level change studies. *Remote Sensing*, 6(3), 2255-2281.

Bouin, M. N., & Wöppelmann, G. (2010). Land motion estimates from GPS at tide gauges: a geophysical evaluation. *Geophysical Journal International*,180(1), 193-209.

Braitenberg, C., Mariani, P., Tunini, L., Grillo, B., & Nagy, I. (2011). Vertical crustal motions from differential tide gauge observations and satellite altimetry in southern Italy. *Journal of Geodynamics*, 51(4), 233-244.

Bretherton, F. P., Davis, R. E., & Fandry, C. B. (1976, July). A technique for objective analysis and design of oceanographic experiments applied to MODE-73. *In Deep Sea Research and Oceanographic Abstracts* (Vol. 23, No. 7, pp. 559-582). Elsevier.

Brown, G. S. (1977). The average impulse response of a rough surface and its applications. Antennas and Propagation, *IEEE Transactions* on, 25(1), 67-74.

Burgette, R. J., Watson, C. S., Church, J. A., White, N. J., Tregoning, P., & Coleman, R. (2013). Characterizing and minimizing the effects of noise in tide gauge time series: relative and geocentric sea level rise around Australia. *Geophysical Journal International*, ggt131.

Cabanes, C., Cazenave, A., & Le Provost, C. (2001). Sea level rise during past 40 years determined from satellite and in situ observations. *Science*, 294(5543), 840-842.

Caccamise, D. J.II, (2003). Sea and land level changes in Hawai'i, *M.S. thesis*, 73 pp., Geology and Geophysics., University of Hawaii, Honolulu.

Caccamise, D.J.II, M. A. Merrifield, M. Bevis, J. Foster, Y. L. Firing, M. S. Schenewerk, F. W. Taylor, and D. A. Thomas (2005), Sea level rise at Honolulu and Hilo, Hawaii: GPS estimates of differential land motion, *Geophysical Research Letters*, 32, L03607.

Calafat, F. M., Chambers, D. P., & Tsimplis, M. N. (2014). On the ability of global sea level reconstructions to determine trends and variability. *Journal of Geophysical Research: Oceans*, 119(3), 1572-1592.

Carrère, L., & Lyard, F. (2003). Modeling the barotropic response of the global ocean to atmospheric wind and pressure forcing-comparisons with observations. *Geophysical Research Letters*, 30(6).

Cartwright, D. E., & Tayler, R. J. (1971). New computations of the tide-generating potential. *Geophysical Journal International*, 23(1), 45-73.

Cartwright, D. E., & Edden, A. C. (1973). Corrected tables of tidal harmonics. *Geophysical Journal International*, 33(3), 253-264.

Cazenave, A., & Nerem, R. S. (2004). Present-day sea level change: Observations and causes. *Reviews of Geophysics*, 42(3).

Cazenave, A. and G. Le Cozannet (2013), Sea level rise and its coastal impacts, *Earth's future,* 2, 15-34, doi: 10.1002/2013EF000188

Chambers, D. P., Mehlhaff, C. A., Urban, T. J., Fujii, D., & Nerem, R. S. (2002). Low-frequency variations in global mean sea level: 1950–2000. *Journal of Geophysical Research: Oceans (1978–2012)*, 107(C4), 1-1.

Chambers, D. P., Merrifield, M. A., & Nerem, R. S. (2012). Is there a 60-year oscillation in global mean sea level?. *Geophysical Research Letters*, 39(18).

Chang, E. T., Chao, B. F., Chiang, C. C., & Hwang, C. (2012). Vertical crustal motion of active plate convergence in Taiwan derived from tide gauge, altimetry, and GPS data. *Tectonophysics*, 578, 98-106.

Chao, B. F., Wu, Y. H., & Li, Y. S. (2008). Impact of artificial reservoir water impoundment on global sea level. *Science*, 320(5873), 212-214.

Chelton, D. B., Ries, J. C., Haines, B. J., Fu, L. L., & Callahan, P. S. (2001). Satellite altimetry. *International Geophysics*, 69, 1-ii.

Chen, Xianyao & Zhang, Xuebin & A. Church, John & Watson, Christopher & King, Matt & Monselesan, Didier & Legresy, Benoit & Harig, Christopher. (2017). The increasing rate of global mean sea-level rise during 1993–2014. *Nature Climate Change*. (7) 492-497. 10.1038/NCLIMATE3325.

Cheng, K. C., Kuo, C. Y., Shum, C. K., Niu, X., Li, R., & Bedford, K. W. (2008). Accurate linking of Lake Erie water level with shoreline datum. *TAO: Terrestrial, Atmospheric, and Oceanic Sciences*, 19, 53.

Cheng, K. C., Kuo, C. Y., Tseng, H. Z., Yi, Y., & Shum, C. K. (2010). Lake surface height calibration of Jason-1 and Jason-2 over the Great Lakes. *Marine Geodesy*, 33(A.1), 186-203.

Cheng, Y., Andersen, O. B., & Knudsen, P. (2012). First evaluation of MyOcean altimetric data in the Arctic Ocean. *Ocean Science Discussions*, 9(1), 291-314.

Cheng, Y., Andersen, O., & Knudsen, P. (2015). An Improved 20-Year Arctic Ocean Altimetric Sea Level Data Record. *Marine Geodesy*, 38(2), 146-162.

Christiansen, B., Schmith, T., & Thejll, P. (2010). A surrogate ensemble study of sea level reconstructions. *Journal of Climate*, 23(16), 4306-4326.

Church, J. A., White, N. J., Coleman, R., Lambeck, K., & Mitrovica, J. X. (2004). Estimates of the regional distribution of sea level rise over the 1950-2000 period. *Journal of climate*, 17(13), 2609-2625.

Church, J. A., & White, N. J. (2006). A 20th century acceleration in global sea-level rise. *Geophysical research letters*, 33(1).

Church, J. A., & White, N. J. (2011). Sea-level rise from the late 19th to the early 21st century. *Surveys in Geophysics*, 32(4-5), 585-602.

Crétaux, J. F., Calmant, S., Romanovski, V., Shabunin, A., Lyard, F., Bergé-Nguyen, M., ... & Perosanz, F. (2009). An absolute calibration site for radar altimeters in the continental domain: Lake Issykkul in Central Asia. *Journal of Geodesy*, 83(8), 723-735.

Dietrich, R. et al. (2001). ITRF coordinates and plate velocities from repeated GPS campaigns in Antarctica. An analysis based on different individual solutions, *J. Geod.*, 74 (10-11), 756-766.

Douglas, B. C. (1991). Global sea level rise. *Journal of Geophysical Research: Oceans (1978–2012)*, 96(C4), 6981-6992.

Douglas, B. C. (1992). Global sea level acceleration. *Journal of Geophysical Research: Oceans (1978–2012)*, 97(C8), 12699-12706.

Douglas, B. C. (1997). Global sea rise: a redetermination. *Surveys in Geophysics*, 18(2-3), 279-292.

Duan, J., Shum, C. K., Guo, J., & Huang, Z. (2012). Uncovered spurious jumps in the GRACE atmospheric de-aliasing data: potential contamination of GRACE observed mass change. *Geophysical Journal International*, 191(1), 83-87.

Ducet, N., Le Traon, P. Y., & Reverdin, G. (2000). Global high-resolution mapping of ocean circulation from TOPEX/Poseidon and ERS-1 and-2. *Journal of Geophysical Research: Oceans (1978–2012)*, 105(C8), 19477-19498.

Eggleston, J., & Pope, J. (2013). Land subsidence and relative sea-level rise in the southern Chesapeake Bay region (No. 1392). US Geological Survey.

Fernandes, M. J., Lázaro, C., Nunes, A. L., & Scharroo, R. (2014). Atmospheric corrections for altimetry studies over inland water. *Remote Sensing*, 6(6), 4952-4997.

Frappart, F., Calmant, S., Cauhopé, M., Seyler, F., & Cazenave, A. (2006). Preliminary results of ENVISAT RA-2-derived water levels validation over the Amazon basin. *Remote Sensing of Environment*, 100(2), 252-264.

Fu, L. L., & Haines, B. J. (2013). The challenges in long-term altimetry calibration for addressing the problem of global sea level change. *Advances in Space Research*, 51(8), 1284-1300.

Garcia, D., Vigo, I., Chao, B. F., & Martinez, M. C. (2007). Vertical crustal motion along the Mediterranean and Black Sea coast derived from ocean altimetry and tide gauge data. *Pure and Applied Geophysics*, 164(4), 851-863.

Gaspar, P., & Ogor, F. (1996). Estimation and analysis of the sea state bias of the new ERS-1 and ERS-2 altimeter data (OPR version 6), *report of task 2, IFREMER contract 96/2.246 002/C, Collect*. Localisation, Satell., Ramonville St. Agne, France.

Gehrels, W. R., & Woodworth, P. L. (2013). When did modern rates of sea-level rise start?. *Global and Planetary Change*, 100, 263-277.

Gornitz, V., & Seeber, L. (1990). Vertical crustal movements along the East Coast, North America, from historic and late Holocene sea level data. *Tectonophysics*, 178(2), 127-150.

Gornitz, V. (2000). Impoundment, groundwater mining, and other hydrologic transformations: impacts on global sea level rise (pp. 97-119). Amsterdam: Academic Press.

Guo, J. Y., Huang, Z. W., Shum, C. K., & van der Wal, W. (2012). Comparisons among contemporary glacial isostatic adjustment models. *Journal of Geodynamics*, 61, 129-137.

Hagedoorn, J. M., & Wolf, D. (2003). Pleistocene and Recent deglaciation in Svalbard: implications for tide-gauge, GPS and VLBI measurements. *Journal of Geodynamics*, 35(4), 415-423.

Haines, B. J., Desai, S. D., & Born, G. H. (2010). The Harvest experiment: Calibration of the climate data record from TOPEX/Poseidon, Jason-1 and the Ocean Surface Topography Mission. *Marine Geodesy*, 33(A.1), 91-113.

Hamlington, B. D., Leben, R. R., Strassburg, M. W., Nerem, R. S., & Kim, K. Y. (2013). Contribution of the Pacific Decadal Oscillation to global mean sea level trends. *Geophysical Research Letters*, 40(19), 5171-5175.

Hamlington, B. D., Leben, R. R., Nerem, R. S., Han, W., & Kim, K. Y. (2011). Reconstructing sea level using cyclostationary empirical orthogonal functions, *Journal of Geophysical Research: Oceans (1978–2012)*, 116(C12).

Hamlington, B. D., S. H. Cheon, P. R. Thompson, M. A. Merrifield, R. S. Nerem, R. R. Leben, and K.-Y. Kim (2016). An ongoing shift in Pacific Ocean sea level, *J. Geophys. Res. Oceans*, 121, 5084–5097,

Hamilton W.C., (1964) Statistics in Physical Sciences - Estimation, hypothesis testing, and least squares. *Ronald Press Company, New York,* 230pp

Hannachi, A. (2007). Pattern hunting in climate: a new method for finding trends in gridded climate data. *International journal of climatology*, 27(1), 1-15.

Holgate, S. J. (2007). On the decadal rates of sea level change during the twentieth century. *Geophysical research letters*, 34(1).

Holgate, S. J., Matthews, A., Woodworth, P. L., Rickards, L. J., Tamisiea, M. E., Bradshaw, E., ... & Pugh, J. (2012). New data systems and products at the permanent service for mean sea level. *Journal of Coastal Research*, 29(3), 493-504.

Houston, J. R., & Dean, R. G. (2011). Sea-level acceleration based on US tide gauges and extensions of previous global-gauge analyses. *Journal of Coastal Research*, 27(3), 409-417.

Hu, R. L., Yue, Z. Q., Wang, L. U., & Wang, S. J. (2004). Review on current status and challenging issues of land subsidence in China. *Engineering Geology*, 76(1), 65-77.

Huang, Z. (2013), The Role of Glaical Isostatic Adjustment (GIA) Process On the Determination of Present-Day Sea-Level Rise, Report. 504, Geodetic Science, The Ohio State University, Columbus, Ohio, USA

Huang, Z., Guo, J. Y., Shum, C. K., Wan, J., Duan, J., Fok, H. S., & Kuo, C. Y. (2013). On the accuracy of glacial isostatic adjustment models for Geodetic Observations to Estimate Arctic Ocean Sea-Level Change. *Terr. Atmos. Ocean. Sci.*, Vol. 24, No. 4, Part I, 471-490

Hudson, D., A. G. Marshall, Y. Yin, O. Alves, and H. H. Hendon, 2013: Improving intraseasonal prediction with a new ensemble generation strategy. *Mon. Wea. Rev*., (141) 4429–4449, doi:10.1175/MWR-D-13-00059.1.

IPCC (2014): Climate Change 2014: Synthesis Report. Contribution of Working Groups I, II and III to the Fifth Assessment Report of the Intergovernmental Panel on Climate Change [Core Writing Team, R.K. Pachauri and L.A. Meyer (eds.)]. IPCC, Geneva, Switzerland, 151 pp.

Iz, H. B. (2006). How do unmodeled systematic mean sea level variations affect long-term sea level trend estimates from tide gauge data?. *Journal of Geodesy*,80(1), 40-46.

Jevrejeva, S., Moore, J. C., Grinsted, A., & Woodworth, P. L. (2008). Recent global sea level acceleration started over 200 years ago?. *Geophysical Research Letters*, 35(8).

Johnson, H. and Agnew, D., (1995). Monument motion and measurements of crustal velocities. *Geophysical Research Letters.* 22(21). 2905-2908

Kaplan, A., Kushnir, Y., & Cane, M. A. (2000). Reduced Space Optimal Interpolation of Historical Marine Sea Level Pressure: 1854-1992*. *Journal of Climate*, 13(16), 2987-3002.

Keihm, S. J., Janssen, M. A., & Ruf, C. S. (1995). TOPEX/Poseidon microwave radiometer (TMR). III. Wet troposphere range correction algorithm and pre-launch error budget. *Geoscience and Remote Sensing, IEEE Transactions on*,33(1), 147-161.

Kemp, A. C., Horton, B. P., Donnelly, J. P., Mann, M. E., Vermeer, M., & Rahmstorf, S. (2011). Climate related sea-level variations over the past two millennia. *Proceedings of the National Academy of Sciences.*

Khan, T. M. A., Quadir, D. A., Murty, T. S., Kabir, A., Aktar, F., & Sarker, M. A. (2002). Relative sea level changes in Maldives and vulnerability of land due to abnormal coastal inundation. *Marine Geodesy*, 25(1-2), 133-143.

Kolker, A. S., Allison, M. A., & Hameed, S. (2011). An evaluation of subsidence rates and sea-level variability in the northern Gulf of Mexico. *Geophysical Research Letters*, 38(21).

Kuo, C. Y., Shum, C. K., Braun, A., & Mitrovica, J. X. (2004). Vertical crustal motion determined by satellite altimetry and tide gauge data in Fennoscandia.*Geophysical Research Letters*, 31(1).

Kuo, C. Y. (2006), Determination and Characterization of 20th Century Global Sea Level Rise, Report. 478, Geodetic Science, The Ohio State University, Columbus, Ohio, USA

Kuo, C. Y., Shum, C. K., Braun, A., Cheng, K. C., & Yi, Y. (2008). Vertical motion determined using satellite altimetry and tide gauges. *Terr. Atmos.*

Kwok, R., & Untersteiner, N. (2011). The thinning of Arctic sea ice. *Phys. Today*, 64(4), 36-41.

Lambeck, K., Esat, T. M., & Potter, E. K. (2002). Links between climate and sea levels for the past three million years. *Nature*, 419(6903), 199-206.

Langbein, J., and Johnson, H. (1997) Correlated errors in geodetic time series: Implications for time-dependent deformation *Journal of Geophysical Research,* 102(B1), 591-603.

Larsen, C. F., Echelmeyer, K. A., Freymueller, J. T., & Motyka, R. J. (2003). Tide gauge records of uplift along the northern Pacific-North American plate boundary, 1937 to 2001. *Journal of Geophysical Research: Solid Earth (1978–2012)*, 108(B4).

Larsen, C. F., Motyka, R. J., Freymueller, J. T., Echelmeyer, K. A., & Ivins, E. R. (2005). Rapid viscoelastic uplift in southeast Alaska caused by post-Little Ice Age glacial retreat. *Earth and Planetary Science Letters*, 237(3), 548-560.

Laxon, S. (1994). Sea ice altimeter processing scheme at the EODC.*International Journal of Remote Sensing*, 15(4), 915-924.

Le Traon, P. Y., Nadal, F., & Ducet, N. (1998a). An improved mapping method of multisatellite altimeter data. *Journal of atmospheric and oceanic technology*,15(2), 522-534.

Le Traon, P. Y., & Ogor, F. (1998b). ERS-1/2 orbit improvement using TOPEX/POSEIDON: The 2cm challenge. *Journal of Geophysical Research-Oceans,* 103(C4), 8045-8057.

Le Traon, P. Y., Faugere, Y., Hernandez, F., Dorandeu, J., Mertz, F., & Ablain, M. (2003). Can we merge GEOSAT Follow-On with TOPEX/POSEIDON and ERS-2 for an improved description of the ocean circulation?. *Journal of Atmospheric and Oceanic Technology*, 20(6), 889-895.

Legresy, B., & Remy, F. (1997). Surface characteristics of the Antarctic ice sheet and altimetric observations. *J. of Glacio*, 43(144), 265-275.

Lemoine, F. G., Zelensky, N. P., Chinn, D. S., Pavlis, D. E., Rowlands, D. D., Beckley, B. D., ... & Luceri, V. (2010). Towards development of a consistent orbit series for TOPEX, Jason-1, and Jason-2. *Advances in space research*,46(12), 1513-1540.

Leuliette, E. W., Nerem, R. S., & Mitchum, G. T. (2004). Calibration of TOPEX/Poseidon and Jason altimeter data to construct a continuous record of mean sea level change. *Marine Geodesy*, 27(1-2), 79-94.

Lidberg, M., Johansson, J. M., Scherneck, H. G., & Milne, G. A. (2010). Recent results based on continuous GPS observations of the GIA process in Fennoscandia from BIFROST. *Journal of Geodynamics*, 50(1), 8-18.

Llovel, W., Cazenave, A., Rogel, P., Lombard, A., & Nguyen, M. B. (2009). Two-dimensional reconstruction of past sea level (1950-2003) from tide gauge data and an Ocean General Circulation Model. *Climate of the Past*, 5(2), 217-227.

Lyard, F., Lefevre, F., Letellier, T., & Francis, O. (2006). Modelling the global ocean tides: modern insights from FES2004. *Ocean Dynamics*, 56(5-6), 394-415.

MacMillan, D. S.;Beckley, B. D.;Fang, P. (2004) Monitoring the TOPEX and Jason - 1 microwave radiometers with GPS and VLBI wet zenith path delays, *Marine Geodesy, Measurement Systems* 27(3/4/05).

Mäkinen, J., & Saaranen, V. (1998). Determination of post-glacial land uplift from the three precise levellings in Finland. *Journal of Geodesy*, 72(9), 516-529.

Masters, D., Nerem, R. S., Choe, C., Leuliette, E., Beckley, B., White, N., & Ablain, M. (2012). Comparison of global mean sea level time series from TOPEX/Poseidon, Jason-1, and Jason-2. *Marine Geodesy*, 35(sup1), 20-41.

Mazzotti, S., Jones, C., & Thomson, R. E. (2008). Relative and absolute sea level rise in western Canada and northwestern United States from a combined tide gauge-GPS analysis. *Journal of Geophysical Research: Oceans (1978–2012),* 113(C11).

Mao, A., C. G. A. Harrison, and T. H. Dixon (1999). Noise in GPS coordinate time series, *Journal. Geophysical Research* 104(B2), 2797–2816.

McIntosh, P. C., J. A. Church, E. R. Miles, K. Ridgway, and C. M. Spillman, 2015: Seasonal coastal sea level prediction using a dynamical model. *Geophys. Res. Lett.*, (42) 6747–6753, doi:10.1002/2015GL065091.

Menke, W., (2012). Geophysical Data Analysis: Discrete Inverse Theory, (Third Edition), *Academic Press*, 330 pp.

Meyssignac, B., Becker, M., Llovel, W., & Cazenave, A. (2012). An assessment of two-dimensional past sea level reconstructions over 1950–2009 based on tide-gauge data and different input sea level grids. *Surveys in Geophysics*, 33(5), 945-972.

Miles, E. R., C. M. Spillman, J. A. Church, and P. C. McIntosh, 2014: Seasonal prediction of global sea level anomalies using an ocean–atmosphere dynamical model. *Climate Dyn*., (43) 2131–2145, doi:10.1007/s00382-013-2039-7

Milly, P. C. D., Cazenave, A., & Gennero, C. (2003). Contribution of climate-driven change in continental water storage to recent sea-level rise. *Proceedings of the National Academy of Sciences,* 100(23), 13158-13161.

Milne, G. A., Davis, J. L., Mitrovica, J. X., Scherneck, H. G., Johansson, J. M., Vermeer, M., & Koivula, H. (2001). Space-geodetic constraints on glacial isostatic adjustment in Fennoscandia. Science, 291(5512), 2381-2385.

Mitchum, G. T. (1994). Comparison of TOPEX sea surface heights and tide gauge sea levels. *Journal of Geophysical Research: Oceans (1978–2012),*99(C12), 24541-24553.

Mitchum, G. T. (1998). Monitoring the stability of satellite altimeters with tide gauges. *Journal of Atmospheric and Oceanic Technology*, 15(3), 721-730.

Mitchum, G. T. (2000). An improved calibration of satellite altimetric heights using tide gauge sea levels with adjustment for land motion. *Marine Geodesy*,23(3), 145-166.

Mitrovica, J. X., Tamisiea, M. E., Davis, J. L., & Milne, G. A. (2001). Recent mass balance of polar ice sheets inferred from patterns of global sea-level change. *Nature*, 409(6823), 1026-1029.

Mitrovica, J. X., Gomez, N., & Clark, P. U. (2009). The sea-level fingerprint of West Antarctic collapse. *Science*, 323(5915), 753-753.

Moore, J. G. (1970). Relationship between subsidence and volcanic load, Hawaii. Bulletin Volcanologique, 34(2), 562-576.

Morris, C. S., & Gill, S. K. (1994). Evaluation of the TOPEX/POSEIDON altimeter system over the Great Lakes. *Journal of Geophysical Research: Oceans (1978–2012)*, 99(C12), 24527-24539.

Munk, W. (2002). Twentieth century sea level: An enigma. Proceedings of the national academy of sciences, 99(10), 6550-6555.

National Geodetic Survey (2001).Technical information Page for G99SSS, GEOID99 and DEFLEC99, http://www.ngs.noaa.gov/GEOID/GEOID99/tech.html. (accessed on November 15, 2006)

Neilan, R.E., J.F. Zumberge, G. Beutler, J. Kouba, (1997). The International GPS Service: A Global Resource for GPS Applications and Research, *Institute of Navigation*, ION GPS-97, 883-889.

Neilan, R.E., (1998). IGS Colleague Directory, IGS Central Bureau, Jet Propulsion Laboratory, Pasadena.

Nerem, R. S., & Mitchum, G. T. (2002). Estimates of vertical crustal motion derived from differences of TOPEX/POSEIDON and tide gauge sea level measurements. *Geophysical Research Letters*, 29(19), 40-1.

Nerem, R. S., Chambers, D. P., Choe, C., & Mitchum, G. T. (2010). Estimating mean sea level change from the TOPEX and Jason altimeter missions. *Marine Geodesy*, 33(A.1), 435-446.

Nerem, R.S., Beckley, B.D., Fasullo, J. T., Hamlington, B. D., Masters, D., Mitchum, G. T. (2018) Climate-change–driven accelerated sea-level rise. *Proceedings of the National Academy of Sciences*, 115(9), 2022-2025.

Nicholls, R. J., & Cazenave, A. (2010). Sea-level rise and its impact on coastal zones. *science*, 328(5985), 1517-1520.

Oschlies, A., & Willebrand, J. (1996). Assimilation of Geosat altimeter data into an eddy-resolving primitive equation model of the North Atlantic Ocean. *Journal of Geophysical Research: Oceans (1978–2012)*, 101(C6), 14175-14190.

Ostanciaux, É., Husson, L., Choblet, G., Robin, C., & Pedoja, K. (2012). Present-day trends of vertical ground motion along the coast lines. *Earth-Science Reviews*, 110(1), 74-92.

Parker, A., Mörner, N.A., Matlack-Klein, P. (2018) Sea level acceleration caused by earthquake induced subsidence in the Samoa Islands, *Ocean & Coastal Management*, 161, 11-19.

Pascual, A., Faugère, Y., Larnicol, G., & Le Traon, P. Y. (2006). Improved description of the ocean mesoscale variability by combining four satellite altimeters. *Geophysical Research Letters*, 33(2).

Peltier, W. R. (2004). Global glacial isostasy and the surface of the ice-age Earth: the ICE-5G (VM2) model and GRACE. *Annu. Rev. Earth Planet. Sci.*, 32, 111-149.

Peterson, B. J., McClelland, J., Curry, R., Holmes, R. M., Walsh, J. E., & Aagaard, K. (2006). Trajectory shifts in the Arctic and subarctic freshwater cycle. *Science*, 313(5790), 1061-1066.

Phien-Wej, N., Giao, P. H., & Nutalaya, P. (2006). Land subsidence in Bangkok, Thailand. Engineering Geology, 82(4), 187-201.

Prandi, P., Ablain, M., Cazenave, A., & Picot, N. (2012). A new estimation of mean sea level in the Arctic ocean from satellite altimetry. *Marine Geodesy*,35(sup1), 61-81.

Press, W. H., (1978). Flicker noises in astronomy and elsewhere. *Comments on Modern Physics, Part C. -Comments on Astrophysics*, 7(4), 103-119.

Proshutinsky, A., Pavlov, V., & Bourke, R. H. (2001). Sea level rise in the Arctic Ocean. *Geophysical Research Letters*, 28(11), 2237-2240.

Proshutinsky, A., Ashik, I. M., Dvorkin, E. N., Häkkinen, S., Krishfield, R. A., & Peltier, W. R. (2004). Secular sea level change in the Russian sector of the Arctic Ocean. *Journal of Geophysical Research: Oceans (1978–2012)*,109(C3).

Permanent Service for Mean Sea Level (PSMSL), 2015, "Tide Gauge Data", Retrieved 21 Sep 2015 from http://www.psmsl.org/data/obtaining/.

Rapp, R. H., Yi, Y., & Wang, Y. M. (1994). Mean sea surface and geoid gradient comparisons with TOPEX altimeter data. *Journal of Geophysical Research: Oceans (1978–2012)*, 99(C12), 24657-24667.

Ray, R. D. (1999). A global ocean tide model from TOPEX/Poseidon altimetry: GOT99. 2. *NASA Tech. Memo*. 209478.

Ray, R. D., Beckley, B. D., & Lemoine, F. G. (2010). Vertical crustal motion derived from satellite altimetry and tide gauges, and comparisons with DORIS measurements. *Advances in Space Research*, 45(12), 1510-1522.

Ray, R. D., & Douglas, B. C. (2011). Experiments in reconstructing twentieth-century sea levels. *Progress in Oceanography,* 91(4), 496-515.

Rudenko, S., Otten, M., Visser, P., Scharroo, R., Schöne, T., & Esselborn, S. (2012). New improved orbit solutions for the ERS-1 and ERS-2 satellites. *Advances in Space Research*, 49(8), 1229-1244.

Saha, S., and Coauthors (2010): The NCEP Climate Forecast System Reanalysis. Bull. *Amer. Meteor. Soc*., (91) 1015–1057, doi:10.1175/2010BAMS3001.1.

Santamaría-Gómez, A., Bouin, M. N., & Wöppelmann, G. (2012). Improved GPS data analysis strategy for tide gauge benchmark monitoring. *In Geodesy for Planet Earth* (pp. 11-18). Springer Berlin Heidelberg.

Santamaría-Gómez, A., Gravelle, M., Collilieux, X., Guichard, M., Míguez, B. M., Tiphaneau, P., & Wöppelmann, G. (2012). Mitigating the effects of vertical land motion in tide gauge records using a state-of-the-art GPS velocity field.*Global and Planetary Change*, 98, 6-17.

Santamaría-Gómez, A., Gravelle, M., & Wöppelmann, G. (2014). Long-term vertical land motion from double-differenced tide gauge and satellite altimetry data. *Journal of Geodesy*, 88(3), 207-222.

Sato, T., Okuno, J. I., Hinderer, J., MacMillan, D. S., Plag, H. P., Francis, O., ... & Fukuda, Y. (2006). A geophysical interpretation of the secular displacement and gravity rates observed at Ny-Ålesund, Svalbard in the Arctic—effects of post-glacial rebound and present-day ice melting. *Geophysical Journal International*, 165(3), 729-743.

Schaeffer, P., Faugere, Y., Legeais, J. F., Ollivier, A., Guinle, T., & Picot, N. (2012). The CNES_CLA.11 global mean sea surface computed from 16 years of satellite altimeter data. *Marine Geodesy*, 35(sup1), 3-19.

Scharroo, R., E. W. Leuliette, J. L. Lillibridge, D. Byrne, M. C. Naeije, and G. T. Mitchum (2013), RADS: Consistent multi-mission products, in Proc. of the Symposium on 20 Years of Progress in Radar Altimetry, Venice, 20-28 September 2012, Eur. Space Agency Spec. Publ., ESA SP-710, p. 4 pp.

Schön, N. (2012). Combining satellite altimetry and GPS-corrected tide gauge data for the reconstruction of sea level anomalies. Doctoral dissertation, Freie Universität Berlin.

Schöne, T., Schön, N., & Thaller, D. (2009). IGS tide gauge benchmark monitoring pilot project (TIGA): scientific benefits. *Journal of Geodesy*, 83(3-4), 249-261.

Sharp Jr, J. M., & Hill, D. W. (1995). Land subsidence along the northeastern Texas Gulf coast: effects of deep hydrocarbon production. *Environmental Geology*, 25(3), 181-191.

Shum, C., Yi, Y., Cheng, K., Kuo, C., Braun, A., Calmant, S., & Chambers, D. (2003). Calibration of JASON-1 altimeter over lake erie special issue: Jason-1 calibration/validation. Marine Geodesy, 26(3-4), 335-354.

Shum, C. K., & Kuo, C. Y. (2011). Observation and geophysical causes of present-day sea-level rise. *In Climate Change and Food Security in South Asia(pp. 85-104)*. Springer Netherlands.

Snay, R., Cline, M., Dillinger, W., Foote, R., Hilla, S., Kass, W., ... & Soler, T. (2007). Using global positioning system-derived crustal velocities to estimate rates of absolute sea level change from North American tide gauge records.*Journal of Geophysical Research: Solid Earth (1978–2012)*, 112(B4).

Sobrero, F.S. (2018). Logarithmic and Exponential Transients in GNSS Trajectory Models as Indicators of Dominant Processes in Post-Seismic Deformation. *The Ohio State University,* M.S. thesis.

Spada, G., & Galassi, G. (2012). New estimates of secular sea level rise from tide gauge data and GIA modelling. *Geophysical Journal International*, 191(3), 1067-1094.

Stammer, D. (2008). Response of the global ocean to Greenland and Antarctic ice melting. *Journal of Geophysical Research: Oceans (1978–2012)*, 113(C6).

Stroeve, J. C., Serreze, M. C., Holland, M. M., Kay, J. E., Malanik, J., & Barrett, A. P. (2012). The Arctic's rapidly shrinking sea ice cover: a research synthesis.*Climatic Change*, 110(3-4), 1005-1027.

Strub, P. T., & James, C. (2002). The 1997–1998 oceanic El Nino signal along the southeast and northeast Pacific boundaries—an altimetric view. Progress in Oceanography, 54(1), 439-458.

Sugiyama, M. (2007), Estimating the economic cost of sea-level rise, Master in Technology and Policy, Massachusetts Institute of Technology, Boston, USA

Tai, C. K., & Wagner, C. (2011). Sampling errors of the global mean sea level derived from TOPEX/Poseidon altimetry. *Acta Oceanologica Sinica*, 30(6), 12-18.

Tamisiea, M. E. (2011). Ongoing glacial isostatic contributions to observations of sea level change. *Geophysical Journal International*, 186(3), 1036-1044.

Timmermann, A., McGregor, S., & Jin, F. F. (2010). Wind effects on past and future regional Sea level trends in the Southern Indo-Pacific*. *Journal of Climate,* 23(16), 4429-4437.

Tran, N., Labroue, S., Philipps, S., Bronner, E., & Picot, N. (2010). Overview and update of the sea state bias corrections for the Jason-2, Jason-1 and TOPEX missions. *Marine Geodesy*, 33(A.1), 348-362.

Trisirisatayawong, I., Naeije, M., Simons, W., & Fenoglio-Marc, L. (2011). Sea level change in the Gulf of Thailand from GPS-corrected tide gauge data and multi-satellite altimetry. *Global and Planetary Change*, 76(3), 137-151.

Tsimplis, M., Spada, G., Marcos, M., & Flemming, N. (2011). Multi-decadal sea level trends and land movements in the Mediterranean Sea with estimates of factors perturbing tide gauge data and cumulative uncertainties. *Global and Planetary Change*, 76(1), 63-76.

Volkov, D. L., & Pujol, M. (2012). Quality assessment of a satellite altimetry data product in the Nordic, Barents, and Kara seas. *Journal of Geophysical Research: Oceans (1978–2012)*, 117(C3).

Wahr, J. M. (1985). Deformation induced by polar motion. *Journal of Geophysical Research: Solid Earth (1978–2012)*, 90(B11), 9363-9368.

Wang, K., Yan Hu, Bevis, M., Kendrick, E., Smalley, R., Barriga, R., Vargas, and Lauria, E., (2007). Crustal motion in the zone of the 1960 Chile earthquake: Detangling earthquake-cycle deformation and forearc-sliver translation, *Geochemistry, Geophysics, Geosystems,* 8(10)

Kelin Wang, Tianhaozhe Sun, Lonn Brown, Ryota Hino, Fumiaki Tomita, Motoyuki Kido, Takeshi Iinuma, Shuichi Kodaira, Toshiya Fujiwara (2018) Learning from crustal deformation associated with the M9 2011 Tohoku-oki earthquake. *Geosphere* ; 14 (2) 552–571

Watson, C., White, N., Burgette, R., Coleman, R., Church, J., & Zhang, J. (2009, June). In Situ calibration results from Bass Strait. *In OSTST meeting*, June (pp. 22-24).

Watson (2015) WATSON 2015 Unabated global mean sea-level rise over the satellite altimeter era

Widlansky, M., Timmermann, A., Cai, W., (2015) Future extreme sea level seesaws in the tropical Pacific. *Science Advances* 1(8), e1500560.

Williams, S. Journal of Geodesy (2003) The effect of coloured noise on the uncertainties of rates estimated from geodetic time series *Journal of Geodesy*, 76(9-10) 483-494

Williams, S. D. P., Y. Bock, P. Fang, P. Jamason, R. M. Nikolaidis, L. Prawirodirdjo, M. Miller, and D. J. Johnson (2004), Error analysis of continuous GPS position time series, *J. Geophys. Res.,* 109(B03412).

Williams, S.D.P. GPS. (2008) CATS: GPS coordinate time series analysis software. *GPS Solns.* 12(2) 147-153.

Willis, J. K., Chambers, D. P., Kuo, C. Y., & Chum, C. K. (2010). Global sea level rise. *Oceanography*, 23(4), 26-35.

Wingham, D. J., Rapley, C. G., & Griffiths, H. (1986). New techniques in satellite altimeter tracking systems. *In ESA Proceedings of the 1986 International Geoscience and Remote Sensing Symposium(IGARSS'86) on Remote Sensing: Today's Solutions for Tomorrow's Information Needs*, (Vol. 3).

Woodworth, P. L. (1990). A search for accelerations in records of European mean sea level. *International Journal of Climatology,* 10(2), 129-143.

Woodworth, P. L., Menéndez, M., & Gehrels, W. R. (2011). Evidence for century-timescale acceleration in mean sea levels and for recent changes in extreme sea levels. Surveys in Geophysics, 32(4-5), 603-618.

Wöppelmann, G., Miguez, B. M., Bouin, M. N., & Altamimi, Z. (2007). Geocentric sea-level trend estimates from GPS analyses at relevant tide gauges world-wide. Global and Planetary Change, 57(3), 396-406.

Wöppelmann, G., Letetrel, C., Santamaria, A., Bouin, M. N., Collilieux, X., Altamimi, Z.,Wiliams, S. D. P. & Miguez, B. M. (2009). Rates of sea-level change over the past century in a geocentric reference frame. *Geophysical Research Letters*,36(12).

Wöppelmann, G., & Marcos, M. (2012). Coastal sea level rise in southern Europe and the nonclimate contribution of vertical land motion. *Journal of Geophysical Research: Oceans (1978–2012)*, 117(C1).

Wöppelmann, G., and M. Marcos (2016) Vertical land motion as a key to understanding sea level change and variability, *Rev. Geophys.*, 54, 64–92.

Wunsch, C., (1972) Bermuda sea level in relation to tides, weather, and baroclinic fluctuations, Revs. Geophys., 10, 1-49.

Wunsch, C., Ponte, R.M., Heimbach, P., (2007) Decadal trends in sea level patterns: 1993–2004. J. Clim. 20 (24), 5889–5911.

Xu, H. (2006). Modification of normalised difference water index (NDWI) to enhance open water features in remotely sensed imagery. *International Journal of Remote Sensing*, 27(14), 3025-3033.

Yi, Y. (1995), Determination of Gridded Mean Sea Surface from TOPEX, ERS-1 and GEOSAT Altimeter Data, Report. 434, Geodetic Science, The Ohio State University, Columbus, Ohio, USA

Yildiz, H., Andersen, O. B., Simav, M., Aktug, B., & Ozdemir, S. (2013). Estimates of vertical land motion along the southwestern coasts of Turkey from coastal altimetry and tide gauge data. *Advances in Space Research*, 51(8), 1572-1580.

Zhang, J., Y. Bock, H. Johnson, P. Fang, S. Williams, J. Genrich, S. Wdowinski, and J. Behr (1997), Southern California permanent GPS geodetic array: Error analysis of daily position estimates and site velocities, *J. Geophys. Res.*, 102(B8), 18035–18055.